

Effect of different emission inventories

T. Amnuaylojaroen et al.

This discussion paper is/has been under review for the journal Atmospheric Chemistry and Physics (ACP). Please refer to the corresponding final paper in ACP if available.

Effect of different emission inventories on modeled ozone and carbon monoxide in Southeast Asia

T. Amnuaylojaroen^{1,2}, M. C. Barth², L. K. Emmons², G. R. Carmichael³,
J. Kreasuwun^{1,4}, S. Prasitwattanaseree⁵, and S. Chantara¹

¹Environmental Science Program and the Center for Environmental Health, Toxicology and Management of Chemical, Chiang Mai University, Faculty of Science, Chiang Mai, Thailand

²Atmospheric Chemistry Division (ACD), National Center for Atmospheric Research (NCAR), Boulder, Colorado USA

³Center for Global and Regional Environmental Research, The University of Iowa, Iowa City, IA, USA

⁴Department of Physics and Materials Science, Faculty of Science, Chiang Mai University, Chiang Mai, Thailand

⁵Department of Statistics, Faculty of Science, Chiang Mai University, Chiang Mai, Thailand

Received: 5 March 2014 – Accepted: 20 March 2014 – Published: 7 April 2014

Correspondence to: T. Amnuaylojaroen (tum@ucar.edu) and M. C. Barth (barthm@ucar.edu)

Published by Copernicus Publications on behalf of the European Geosciences Union.

Title Page

Abstract

Introduction

Conclusions

References

Tables

Figures

◀

▶

◀

▶

Back

Close

Full Screen / Esc

Printer-friendly Version

Interactive Discussion



Abstract

In order to improve our understanding of air quality in Southeast Asia, the anthropogenic emissions inventory must be well represented. In this work, we apply different anthropogenic emission inventories in the Weather Research and Forecasting Model with Chemistry (WRF-Chem) version 3.3 using MOZART gas-phase chemistry and GOCART aerosols to examine the differences in predicted carbon monoxide (CO) and ozone (O₃) surface mixing ratios for Southeast Asia in March and December 2008. The anthropogenic emission inventories include the Reanalysis of the TROpospheric chemical composition (RETRO), the Intercontinental Chemical Transport Experiment-Phase B (INTEX-B), the MACCity emissions (adapted from the Monitoring Atmospheric Composition and Climate and megacity Zoom for the Environment projects), the Southeast Asia Composition, Cloud, Climate Coupling Regional Study (SEAC4RS) emissions, and a combination of MACCity and SEAC4RS emissions. Biomass burning emissions are from the Fire Inventory from NCAR (FINNv1) model. WRF-chem reasonably predicts the 2 m temperature, 10 m wind, and precipitation. In general, surface CO is underpredicted by WRF-Chem while surface O₃ is overpredicted. The NO₂ tropospheric column predicted by WRF-Chem has the same magnitude as observations, but tends to underpredict NO₂ column over the equatorial ocean and near Indonesia. Simulations using different anthropogenic emissions produce only a slight variability of O₃ and CO mixing ratios, while biomass burning emissions add more variability. The different anthropogenic emissions differ by up to 20 % in CO emissions, but O₃ and CO mixing ratios differ by ~ 4.5 % and ~ 8 %, respectively, among the simulations. Biomass burning emissions create a substantial increase for both O₃ and CO by ~ 29 % and ~ 16 %, respectively, when comparing the March biomass burning period to December with low biomass burning emissions. The simulations show that none of the anthropogenic emission inventories are better than the others and any of the examined inventories can be used for air quality simulations in Southeast Asia.

Effect of different emission inventories

T. Amnuaylojaroen et al.

Title Page

Abstract

Introduction

Conclusions

References

Tables

Figures

◀

▶

◀

▶

Back

Close

Full Screen / Esc

Printer-friendly Version

Interactive Discussion



1 Introduction

Southeast Asia, which includes the Indochina peninsula and the Indonesian archipelago, can have significant air quality problems. Understanding the contribution of different sources of tropospheric ozone (O_3) and its precursors, carbon monoxide (CO) and nitrogen oxides ($NO_x = NO + NO_2$), for Southeast Asia provides valuable information on maintaining good air quality for both human well-being and ecosystems. Previous studies examining air pollutants and their sources via regional model simulations have focused primarily on China (e.g. Wang et al., 2005; Geng et al., 2011), East Asia (Han et al., 2008; Tanimoto et al., 2009), and India (Adhikary et al., 2007; Kumar et al., 2012; Ghude et al., 2013). Here, we examine the effect of different emission inventories on modeled surface O_3 and CO for Southeast Asia, a region generally ignored in previous studies.

Previous studies have indicated that both local anthropogenic and biomass burning emissions, as well as emissions upstream are important for local ozone air quality in Asia. In East Asia, Tanimoto et al. (2009) noted relatively small changes in decadal O_3 trends at sites near the Japanese coast, but a larger increase in measured O_3 at a remote mountainous site in Japan. Using a regional chemistry transport model, Tanimoto et al. (2009) attributed half of the observed increase at the mountainous site to increasing anthropogenic emissions in Asia. The results from this study suggested that the actual growth in emissions between 1998–2007 was significantly underestimated. Using a nested eastern Asia domain within a global chemistry transport model, Wang et al. (2011) found that local sources of O_3 precursors produced much of the O_3 in the region; however, O_3 transported from Europe, North America, India and South-east Asia also impacted O_3 concentrations in eastern China depending on the season. Liu et al. (2008), using a regional air quality model, determined that fossil fuel and biomass burning emissions from East Asia increased surface CO and O_3 in Taiwan by 70–150 % and 50–100 %, respectively, compared to model results that excluded background emissions. They attributed up to 20 % of the surface CO and O_3 in Taiwan to

ACPD

14, 9345–9400, 2014

Effect of different emission inventories

T. Amnuaylojaroen et al.

Title Page

Abstract

Introduction

Conclusions

References

Tables

Figures

◀

▶

◀

▶

Back

Close

Full Screen / Esc

Printer-friendly Version

Interactive Discussion



biomass burning emissions from Eastern China. Both the aerosol optical depth and O_3 concentrations in the Pearl River Delta were also found to be affected by biomass burning emissions occurring upstream in Southeast Asia (Deng et al., 2008).

Southeast Asia is subject to the effluent of pollution from the main continent, yet the region itself is rapidly growing and has increasing anthropogenic and biomass burning emissions, which are especially high during the dry season (November–April). To simulate ozone production and concentrations in Southeast Asia, realistic estimates of emissions from both local and regional sources, including fossil fuel use, other anthropogenic activities, and biomass burning, must be available. Emission inventories for Asia have been developed by several groups (e.g., Akimoto and Narita, 1994; Streets et al., 2003; Ohara et al., 2007; Zhang et al., 2009; Kurokawa et al., 2013) for both chemistry-climate and air quality studies. For example, the REanalysis of the TROpospheric chemical composition (RETRO) and the Emission Database for Global Atmospheric Research (EDGAR) emissions inventories (Olivier et al., 2005; Schultz et al. 2007) are global emissions inventories developed for chemistry-climate studies. Streets et al. (2003) developed a 2001 emission inventory for the ACE-Asia (Asian Pacific Regional Aerosol Characterization Experiment) and TRACE-P (Transport and Chemical Evolution over the Pacific) field campaigns that took place in the East Asian and Western Pacific region during spring 2001. Zhang et al. (2009) developed a 2006 emissions inventory for Asia to support the Intercontinental Chemical Transport Experiment-Phase B (INTEX-B) field campaign. The INTEX-B field campaign emphasized China emissions because they dominate the Asia pollutant outflow to the Pacific. Ohara et al. (2007) developed the Regional Emission inventory in Asia (REAS) for 1980–2020 in order to conduct air quality studies for recent past, present day, and near future time periods. More recently, Kurokawa et al. (2013) released REAS version 2.1, providing updated emissions for each year from 2000 to 2008 for Asian countries east of $\sim 55^\circ$ E. The MACCity emissions inventory (Granier et al., 2011), which is an outcome from two European Commission projects (MACC and CityZen), is a 1980–2010 global emissions inventory for chemistry-climate studies. Most recently the South-

Effect of different emission inventories

T. Amnuaylojaroen et al.

Title Page

Abstract

Introduction

Conclusions

References

Tables

Figures

◀

▶

◀

▶

Back

Close

Full Screen / Esc

Printer-friendly Version

Interactive Discussion



Effect of different emission inventories

T. Amnuaylojaroen et al.

Title Page

Abstract

Introduction

Conclusions

References

Tables

Figures

◀

▶

◀

▶

Back

Close

Full Screen / Esc

Printer-friendly Version

Interactive Discussion



east Asia Composition, Clouds and Climate Coupling by Regional Study (SEAC4RS) emissions inventory (Lu and Streets, 2012) for 2012 emissions has been released for field campaign support. Four emission inventories, RETRO, INTEX-B, MACCity and SEAC4RS, will be described in more detail in Sect. 3.

Although emission inventories (anthropogenic, biomass burning and biogenic emissions) are important inputs for air quality models and regulatory control strategy development, there have been only a few studies (e.g. Ohara et al., 2007) that compare the emission inventories and their uncertainties on simulated surface CO and O₃ mixing ratios in Asia. Here, we apply the Weather and Forecasting Model coupled with Chemistry (WRF-Chem) to examine the variability of predicted O₃ and CO surface mixing ratios in Southeast Asia when five different anthropogenic emission inventories (RETRO, INTEX-B, MACCity, SEAC4RS, and a modified SEAC4RS) are used as inputs. Results from this comparison are presented for a low biomass burning period (December) and a high biomass burning period (March).

We begin this manuscript by describing the model configuration (Sect. 2) and emission inventories (Sect. 3) applied in the model simulations. We then evaluate the model results (Sect. 4) with available datasets. In Sect. 5, we compare the surface O₃ and CO predictions among the different simulations in order to quantify the variability produced by the different emission inventories.

2 Model description and configuration

We use the Weather Research Forecasting Model (Skamarock et al., 2008) coupled with Chemistry (WRF-Chem version 3.3) to investigate the variation of O₃ and CO predictions among different anthropogenic emissions inventories for Southeast Asia. The WRF-Chem model is a new-generation regional air quality model (Grell et al., 2005; Fast et al., 2006) that shares the meteorology and chemistry routines, the same land surface schemes, time-transport schemes, vertical mixing parameterizations, and time steps for transport and vertical mixing.

Effect of different emission inventories

T. Amnuaylojaroen et al.

Title Page

Abstract

Introduction

Conclusions

References

Tables

Figures

◀

▶

◀

▶

Back

Close

Full Screen / Esc

Printer-friendly Version

Interactive Discussion



For this study, one model domain was configured to cover the entire area of South-east Asia (SEA) and a part of China and India (Fig. 1). The model was run with a horizontal grid spacing of 36 km and 51 vertical levels from the surface to 10 hPa. The vertical grid spacing stretched from ~ 60 m near the surface to ~ 700 m near the tropopause. The initial and boundary conditions were from NCEP Final Analysis (FNL) $1^\circ \times 1^\circ$ data for meteorological variables, which include winds, potential temperature, pressure, and water vapor. These variables and condensed water (i.e., cloud particles), and chemistry species were integrated forward in time using a Runge–Kutta integration method. The moisture variables and chemistry species were advected using a monotonic scheme (Wang et al., 2009). Grid nudging (Stauffer and Seaman, 1990) was employed for the horizontal wind, temperature and water vapor for all vertical levels to ensure the accuracy of the large-scale meteorology during the month of simulation. The nudging coefficients for all variables were set to be 0.0003 s^{-1} , and nudging was performed every 6 h, consistent with the timing of the FNL data.

The model set-up used the following modules and parameterizations. Cloud physics was represented by the Thompson et al. (2004) parameterization, which predicts the mass mixing ratio for rain, snow, and graupel and mass and number of cloud water and cloud ice. The Grell-3 scheme, based on the Grell and Devenyi (2002) scheme, was used for the parameterization of sub-grid convection. The planetary boundary layer was parameterized with the Mellor–Yamada–Janjic (MYJ) scheme (Janjic, 2002) and the Noah land surface model (Chen and Dudhia, 2001) was used to provide heat and moisture fluxes over land. For heating rates, the Goddard scheme (Chou and Suarez, 1994) was used for short wave radiation and the Rapid Radiative Transfer Model (Mlawer et al., 1997) was used for long wave radiation. Feedbacks between aerosols and the radiation scheme were not included in any simulations.

Initial and boundary conditions for the chemical species were provided by the global chemistry Model for Ozone and Related Chemical Tracers, version 4 (MOZART4; Emmons et al., 2010) 6-hourly output. MOZART4 includes 84 gas-phase species, 12 bulk aerosol compounds, 39 photolysis and 127 gas-phase reactions. In our WRF-Chem

Effect of different emission inventories

T. Amnuaylojaroen et al.

Title Page

Abstract

Introduction

Conclusions

References

Tables

Figures

I◀

▶I

◀

▶

Back

Close

Full Screen / Esc

Printer-friendly Version

Interactive Discussion



simulations, gas-phase chemistry was represented by the MOZART chemistry mechanism and aerosols by the GOCART representation (Chin et al., 200). A kinetic pre-processor and Rosenbrock solver (Sandu et al., 2006) was applied. The photolysis rates were computed using fast-TUV (Tie et al., 2003), which modifies the photolysis rates based on the presence of aerosols and clouds in each model grid cell. Dry deposition of gases and aerosols followed the Wesely (1989) resistance method. Wet deposition of soluble gases was calculated using the method described by Neu and Prather (2012).

Emissions from biomass burning, undisturbed vegetation, and anthropogenic sources were included in the simulations. The Fire Inventory from NCAR (FINN) model (Wiedinmyer et al., 2010) provided daily, 1 km resolution, global estimates of trace gas and particulate emissions from open burning including wildfires, agricultural fires, and prescribed burning for all the simulations conducted. Biofuel use and trash burning were not included in the FINN emission estimates. Biogenic emissions were computed online by the Model of Emissions of Gases and Aerosols from Nature (MEGAN) Version 2.04 (Guenther et al., 2006), which uses WRF-predicted temperature and downward radiation for its calculations. The anthropogenic emission inventories used as inputs to the WRF-Chem simulations are described in Sect. 3.1.

3 Emissions

In this study we perform WRF-Chem simulations with four different anthropogenic emission inventories, consisting of RETRO, INTEX-B, MACCity and SEAC4RS, and an inventory combining MACCity and SEAC4RS emissions. The simulations also include biogenic emissions (MEGAN v2.04) and biomass burning (FINNV1) emissions, which were the same in all simulations. Different groups have compiled the different anthropogenic emission inventories for different years: RETRO for 2000, INTEX-B for 2006, MACCity for 2010 and SEAC4RS for 2012. Due to these differences, the total emissions and associated uncertainties for the region are variable. The five emission inventories

were applied to (1) evaluate surface CO and O₃ predictions with monitoring station observations, and (2) determine the extent the model predictions are limited by variations in the emissions inventories.

3.1 Description of the anthropogenic emission inventories

The RETRO project aimed at analyzing the long-term changes in the atmospheric budget of trace gases and aerosols over the time period from 1960 to 2000. The RETRO anthropogenic emissions (Schultz et al., 2007) are derived from a preliminary version of the TNO (Netherlands Organization for Applied Scientific Research) emissions, for the 1960–2000 time period with spatial resolution of 0.5° × 0.5°. The anthropogenic emissions in the RETRO inventory include only combustion sources (Granier et al., 2011). Schultz et al. (2007) report several uncertainties associated with the RETRO emissions. These uncertainties include omission of specific sectors (e.g. railway traffic or cement manufacturing), underestimation of CO combustion emissions and NO_x ship traffic emissions, and the lack of weekly and diurnal profiles of emissions. For the Southeast Asia region the RETRO seasonal cycle is based on what was developed for Europe, but has a reduced amplitude. Kurokawa et al. (2013) show that there is very little seasonal cycle for anthropogenic emissions of NO_x and black carbon over India, which is a region similar to Southeast Asia in terms of climate. The RETRO inventory provided regional information for the emissions of a variety of non-methane volatile organic compounds (NMVOCs) including ethane, propane, butanes, pentanes, hexanes and higher alkanes, ethene, propene, ethyne, other alkenes and alkynes, benzene, toluene, xylene, trimethyl benzenes and other aromatics, organic alcohols, esters, ethers, chlorinated hydrocarbons, formaldehyde and other aldehydes, ketones, organic acids, and other VOCs.

As part of the INTEX-B field campaign, which was conducted by the National Aeronautics and Space Administration (NASA) in spring 2006, anthropogenic emissions were developed for the specific year and season as the field campaign (Zhang et al., 2009). The emissions are estimated for eight major chemical species, sulfur dioxide

Effect of different emission inventories

T. Amnuaylojaroen et al.

Title Page

Abstract

Introduction

Conclusions

References

Tables

Figures

◀

▶

◀

▶

Back

Close

Full Screen / Esc

Printer-friendly Version

Interactive Discussion



Effect of different emission inventories

T. Amnuaylojaroen et al.

(SO₂), NO_x, CO, NMVOCs, PM₁₀, PM_{2.5}, black carbon (BC) and organic carbon (OC), with a spatial resolution of 0.5° × 0.5°. To represent the individual VOCs represented in the MOZART mechanism, the NMVOC emissions are speciated based on the ratios of the individual VOC to the total NMVOCs derived from the RETRO inventory. That is, the individual VOC fraction from the RETRO inventory is multiplied with the total INTEX-B NMVOC to get the individual VOC emissions. The uncertainty of the INTEX-B emissions for the Southeast Asian countries is estimated to be similar to the TRACE-P emissions uncertainty (Zhang et al., 2009), e.g. ±37 % for NO_x emissions and ±185 % for CO emissions. The INTEX-B emissions uncertainties for China are smaller (±31 % for NO_x and ±70 % for CO).

The MACCity emissions (Granier et al., 2011) are an outcome of two European Commission projects, MACC (Hollingsworth et al., 2008) and CityZen (<http://cityzen-project.eu>) and are an extension of the ACCMIP historical emissions dataset (Lamarque et al., 2010). The goal of the MACCity emissions inventory is to support the IPCC-AR5 (Intergovernmental Panel for Climate Change Assessment Report 5), providing historical emissions on a decadal basis from 1960 to 2020, as well as for future emissions scenarios based on RCPs (Representation Concentration Pathways; van Vuuren et al., 2011). Anthropogenic emissions have been interpolated on a yearly basis between the base years 1990, 2000, 2005 and 2010. The MACCity emissions are estimated for 19 chemical species: CO, ethane, ethene, propane, propene, butane and higher alkanes, butene and higher alkenes, methanol, other alcohols, formaldehyde, other aldehydes, acetone, other ketones, total aromatics, ammonia, NO_x, SO₂, BC, and OC, with spatial resolution of 0.5° × 0.5°. Because the 2000 MACCity emissions inventory does not have substantial biases compared to other emissions inventories, it is expected that the 2010 MACCity emissions inventory has uncertainties similar to those discussed by Lamarque et al. (2010, and references therein), which can be on the order of a factor of 2. In this study, we use the 2010 emissions estimates from MACCity, which are based on the RCP8.5 scenario.

Title Page

Abstract

Introduction

Conclusions

References

Tables

Figures

◀

▶

◀

▶

Back

Close

Full Screen / Esc

Printer-friendly Version

Interactive Discussion



**Effect of different
emission inventories**

T. Amnuaylojaroen et al.

The SEAC4RS emissions inventory (Lu and Streets, 2012), which is a regional anthropogenic emission dataset prepared for the NASA SEAC4RS field campaign and for the Asia region, represents an update of the TRACE-P emissions (Streets et al., 2003). These emissions are appropriate for year 2012 and include four emissions sectors: residential, industry, power and transport. There are 10 major chemical species, CH₄, CO, NO_x, NMVOC, CO₂, SO₂, PM₁₀, PM_{2.5}, BC and OC, with spatial resolution of 0.1° × 0.1°. Not only does this emissions inventory provide a finer resolution than the other inventories applied in this study, the SEAC4RS emissions data include an update of the Asia emission estimates using new energy use data and updated emission factors (both reflecting the year 2012), as well as the development of a new emission inventory for Southeast Asia using a technology-based methodology, which is the first detailed emission update for the region since TRACE-P. Similar to the INTEX-B inventory described above, the total NMVOC emissions were speciated to the individual VOC species of the MOZART-4 mechanism using fractions derived from the RETRO inventory.

In addition to the four inventories described above, we have conducted a simulation with a combined MACCity/SEAC4RS emissions inventory, which replaces MACCity with the SEAC4RS emissions over Asia and includes the MACCity ship emissions. In the MACCity emissions inventory, ship emissions account for 15 % of the NO emissions and 0.1 % of the CO emissions. To ensure consistency in this simulation, the SEAC4RS emissions have been regridded from 0.1° × 0.1° resolution to 0.5° × 0.5°. This regridding causes differences between the SEAC4RS-only and MACCity/SEAC4RS emissions outside the shipping regions in the model domain.

While both the RETRO and MACCity emission inventories have monthly temporal variability, the INTEX-B and SEAC4RS inventories are annual totals. A monthly profile was created from the RETRO emissions, where the fraction of the annual emissions assigned to each month ($Frac_{Monthly}$) was calculated from the ratio of the RETRO monthly emissions ($RETRO_{Monthly}$) to the RETRO annual emissions ($RETRO_{Annual}$). The monthly fraction was then multiplied by the annual emissions of both the INTEX-B

[Title Page](#)[Abstract](#)[Introduction](#)[Conclusions](#)[References](#)[Tables](#)[Figures](#)[◀](#)[▶](#)[◀](#)[▶](#)[Back](#)[Close](#)[Full Screen / Esc](#)[Printer-friendly Version](#)[Interactive Discussion](#)

and SEAC4RS inventories to estimate the monthly emissions. This procedure is described by the following equations:

$$\text{RETRO}_{\text{Annual}} = \sum_{i=1}^{12} \text{RETRO}_{\text{Monthly}} \quad (1)$$

$$\text{Frac}_{\text{Monthly}}(i) = \frac{\text{RETRO}_{\text{Monthly}}(i)}{\text{RETRO}_{\text{Annual}}} \quad (2)$$

$$\text{Emission}_{\text{Monthly}}(i) = \text{Frac}_{\text{Monthly}}(i) \times \text{Emission}_{\text{Annual}} \quad (3)$$

where the $\text{Emission}_{\text{Monthly}}$ is the monthly emissions for the INTEX or SEAC4RS inventory and $\text{Emission}_{\text{Annual}}$ is the annual emissions from the INTEX or SEAC4RS inventory.

3.2 Emission comparison

The monthly-average emissions from the five different anthropogenic emissions inventories and the biomass burning emissions calculated by the FINN model for CO and NO_x are compared for both March and December in Figs. 1–4. The sum of these emissions over the entire model domain is listed in Table 1. In March, the biomass burning sources dominate the emissions of CO and NO_x. The biomass burning occurs primarily over the Indochina peninsula and Southeast China where CO biomass burning emissions dominate the inventory. In March in Southeast Asia, ~ 70 % of the total CO emissions is from biomass burning and only ~ 30 % is from anthropogenic emissions. This partitioning is true for all the emission inventories applied in this study. In December, the biomass burning emissions are much smaller.

Anthropogenic emissions of CO vary between emissions inventories, with RETRO and MACCity emissions having higher values, particularly in northeast India and southeast China. Over the entire domain, the anthropogenic NO_x emissions are quite similar between RETRO, INTEX-B, MACCity, and MACCity/SEAC4RS emissions, but are much smaller in the SEAC4RS inventory, since this inventory alone does not include

Title Page

Abstract

Introduction

Conclusions

References

Tables

Figures

◀

▶

◀

▶

Back

Close

Full Screen / Esc

Printer-friendly Version

Interactive Discussion



ship emissions. By comparing RETRO emissions to SEAC4RS emissions, the total anthropogenic emissions in Southeast Asia increased by ~ 24 % for CO and by ~ 51 % for NO_x between 2000 and 2012.

Comparison of the total CO emissions from the various inventories across Southeast Asia (Table 1) show that in March, the RETRO inventory is within ±5 % of the INTEX-B and MACCity inventories, but is ~ 20 % greater than the MACCity/SEAC4RS and SEAC4RS inventories. In December, the CO MACCity/SEAC4RS inventory is 35 % lower than the RETRO emissions inventory. The SEAC4RS NO emissions are substantially less (~ 45 %) than the other inventories in both March and December because of the lack of ship emissions in the SEAC4RS inventory. NO emissions in the INTEX-B and MACCity inventories are similar to each other and ~ 10 % lower than the RETRO emissions. In December, the INTEX-B, MACCity and MACCity/SEAC4RS NO emissions are similar and are ~ 25 % lower than the RETRO inventory.

The emissions used in our study are consistent with Ohara et al. (2007) for CO emissions, but there are differences for NO emissions. Ohara et al. (2007) concluded that the Asian CO emissions for 2000 were higher than the CO emissions reported in other emission inventories including TRACE-P, EDGAR and IIASA. However, REAS v2.1 (Kurakawa et al., 2013) CO emissions are lower than REAS v1 and are similar to TRACE-P emissions for 2000. Our results also show that the total CO emissions estimated by RETRO for 2000 were higher than the CO emissions in the INTEX-B, MACCity, and SEAC4RS inventories, which are appropriate for 2006, 2010 and 2012, respectively. The total NO emission from other inventories including INTEX-B, MACCity, and SEAC4RS tend to be smaller than the RETRO emissions, while Ohara et al. (2007) show REAS NO emissions were about the same as IIASA, smaller than TRACE-P, and larger than EDGAR NO emissions. The more recent REAS v2.1 inventory has NO_x emissions lower than the REAS v1 inventory but is similar to TRACE-P for year 2000 and less than INTEX-B for year 2006. While Ohara et al. (2007) used the same year for comparison to other inventories, our study uses emission inventories for different years.

Effect of different emission inventories

T. Amnuaylojaroen et al.

Title Page

Abstract

Introduction

Conclusions

References

Tables

Figures

◀

▶

◀

▶

Back

Close

Full Screen / Esc

Printer-friendly Version

Interactive Discussion



4 Data used for the model evaluation

To evaluate the ability of the WRF-Chem model to represent the meteorology and chemical composition over Southeast Asia during March and December 2008, the model results are evaluated with observations. The data used for the model evaluation is described here.

4.1 Meteorology data description

The predicted meteorology from the WRF simulations, which is the same for all model simulations, was evaluated by comparing 2 m temperature, 10 m winds, and precipitation with existing observations. The observations used for this evaluation include the Modern-Era Retrospective Analysis For Research And Applications (MERRA) products, the Tropical Rainfall Measuring Mission (TRMM) satellite data, and data from the Global Precipitation Climatology Center (GPCC).

The MERRA product (Rienecker et al., 2011) is generated using Version 5.2.0 of the GEOS-5 DAS (Goddard Earth Observing System Model Data Assimilation System) with the model and analysis each at about $0.5^\circ \times 0.6^\circ$ resolution. MERRA has complete analysis of over 30 years (from 1979 to present) of data. The 2 m temperature and 10 m winds produced by the MERRA analysis system are hourly. However, the provided monthly-averaged data were used here to evaluate the WRF results.

The main objective of the TRMM satellite (Huffman et al., 1997), which is a joint mission between the NASA and Japan Aerospace Exploration Agency (JAXA), is to monitor rainfall in the tropics. We compare the WRF-Chem monthly surface rainfall to the TRMM product that is a combination of instruments, including the Precipitation Radar and TRMM Microwave Imager, allowing us to compare model results with the high-resolution data from the Precipitation Radar filled in by data from the TRMM Microwave Imager. The precipitation gauge analysis is used to correct any biases in the satellite data (Huffman and Bolvin, 2012).

Title Page

Abstract

Introduction

Conclusions

References

Tables

Figures

◀

▶

◀

▶

Back

Close

Full Screen / Esc

Printer-friendly Version

Interactive Discussion



Effect of different emission inventories

T. Amnuaylojaroen et al.

Title Page

Abstract

Introduction

Conclusions

References

Tables

Figures

◀

▶

◀

▶

Back

Close

Full Screen / Esc

Printer-friendly Version

Interactive Discussion



Monthly precipitation from the GPCC dataset (Schneider et al., 2011b; Rudolf and Schneider, 2005) is obtained from global station data that are gridded onto a $1^\circ \times 1^\circ$ global domain. The GPCC monthly precipitation product is based on anomalies from the climatological mean at each station. The anomalies are spatially interpolated by using a modified version of the robust empirical interpolation method SPHEREMAP. The method constitutes a spherical adaptation (Willmott et al., 1985) of Shepard's empirical weighting scheme (Shepard, 1968; Schneider et al., 2011a).

4.2 Chemistry data description

Observations from four measurement platforms are used to evaluate the WRF-Chem predictions of CO , O_3 and NO_2 : a ground-based monitoring network in Thailand, ozonesondes in the Southeast Asia region, Version 6 Measurement of Pollution In the Troposphere (MOPITT) satellite instrument, and the Ozone Monitoring Instrument (OMI) satellite instrument. The ground-based chemistry observations in Thailand are provided by the Thai Pollution Control Department (PCD). The Thai PCD monitors the hourly surface concentrations of five chemical species: O_3 , CO , NO_2 , SO_2 and PM_{10} at six locations (Fig. 5g). The measurement sites in Thailand are located in urban areas and therefore are dominated by urban (especially motor vehicles) emissions. These data are measured by using the “reference method” or “equivalent methods”. Almost all O_3 observation instruments are from Teledyne Advanced Pollution Instrumentation Model 400 (<http://www.teledyne-api.com/products/400e.asp>). The instrument has a lower detection limit of 0.6 ppbv and a precision of 1 %. Almost all CO observation instruments are from Teledyne Advanced Pollution Instrumentation Model 300 (<http://www.teledyne-api.com/products/300e.asp>), which has a lower detection limit of 40 ppbv and a precision of 0.5 %. The PCD measurements periodically have missing data, but the missing data are only $\sim 15\%$ of the time.

The SHADOZ ozonesonde network (Thompson et al., 2012) was initiated to provide vertical profiles of ozone in the tropics for satellite data verification, model evaluation, and insights into tropical chemistry and dynamics. SHADOZ has collected more than

Effect of different emission inventories

T. Amnuaylojaroen et al.

Title Page

Abstract

Introduction

Conclusions

References

Tables

Figures

◀

▶

◀

▶

Back

Close

Full Screen / Esc

Printer-friendly Version

Interactive Discussion



3000 ozone profiles from 14 sites in tropical and subtropical regions using balloon-borne electrochemical concentration cell (ECC) ozone detectors flown with standard radiosondes. It is estimated that the accuracy and precision of the ozone measurement is 5 %, but biases can be found with individual stations. Ozonesondes from three stations, Kuala Lumpur, Malaysia, Hanoi, Vietnam, and Watukosek, Java (Fig. 5g), are used in the model evaluation presented in this manuscript. Total ozone column at these stations can be 5–10 % lower than total ozone measured by the OMI satellite instrument (Thompson et al., 2012).

Satellite observations are quite valuable for model evaluation, but require careful interpretation to be used quantitatively. In many cases (as in MOPITT CO and OMI NO₂) the retrieved mixing ratios or column densities can be expressed as a linear combination of the true atmospheric profile (x) and a priori information (x_a), balanced according to the averaging kernels (\mathbf{A}) (\mathbf{I} is the identity matrix):

$$x_{\text{ret}} = \mathbf{A}x + (\mathbf{I} - \mathbf{A})x_a \quad (4)$$

The averaging kernels represent the sensitivity of the retrievals to the actual concentration profiles, and vary in time and space depending on the temperature profile, the thermal contrast between air and surface temperatures, the concentration profile and surface emissivity.

The MOPITT Version 6 carbon monoxide retrievals (Deeter et al., 2012) use both near-infrared and thermal-infrared observations simultaneously to enhance the retrieval sensitivity of CO in the lower troposphere. This feature is important to air quality analyses and studies of CO sources. The V5 MOPITT surface-level CO validation shows biases on the order of a few percent, and V6 is very similar (Deeter et al., 2012).

The OMI Level-3 Global Gridded NO₂ data product, archived at the NASA Goddard Earth Sciences Data and Information Service Center (GES DISC), has a spatial resolution of about 13 km × 24 km at nadir in normal operational mode. OMI measures the backscattered radiation over the 0.27–0.5 μm wavelength range to obtain the total column of trace species, such as NO₂, O₃, formaldehyde, SO₂ and aerosols. The

Effect of different emission inventories

T. Amnuaylojaroen et al.

Title Page

Abstract

Introduction

Conclusions

References

Tables

Figures

◀

▶

◀

▶

Back

Close

Full Screen / Esc

Printer-friendly Version

Interactive Discussion



5 tropospheric NO₂ column retrieval algorithm follows Bucselá et al. (2006) who use the DOAS methodology, air mass factors, and typical NO₂ profiles from chemical transport models to obtain the vertical column density. The OMI tropospheric NO₂ column data have been shown to have a good correlation with INTEX-B aircraft measurements
10 (Boersma et al., 2008). Good agreement of OMI tropospheric NO₂ column has also been found with MAX-DOAS ground-based measurements (Kramer et al., 2008). However, some recent studies have suggested that the OMI retrieval has a positive bias of 0–30 % (e.g., Boersma et al., 2009; Zhou et al., 2009). To evaluate NO₂ from model results, we compare the tropospheric column of NO₂ from the OMI Level-3 Global Grid-
15 ded NO₂ data product with WRF-Chem NO₂ columns that have been adjusted using the averaging kernel and a priori information (Eq. 4) provided with the data product (e.g., Emmons et al., 2004).

5 Model results and evaluation

5.1 Meteorology evaluation

15 Monthly-averaged 2 m temperature, wind speed and direction are compared to the MERRA reanalysis dataset. In general, the model-predicted temperature agrees well with the MERRA output (Fig. 5) for the March 2008 simulation, although some regions, e.g. Indochina peninsula, have 2–3 °C lower temperatures than the monthly-averaged reanalysis output. The WRF-predicted wind speed pattern is similar to the MERRA
20 output for March. However, the wind speed is over-predicted in the South China Sea by ~ 2 ms⁻¹. The wind direction agrees quite well with MERRA output (Fig. 5e and f). For December 2008 (not shown), the simulated 2 m temperature, 10 m wind speed and wind direction, in general, also agree well with the MERRA output; however, the temperature is slightly under-predicted over land and the wind speed is over-predicted
25 over the South China Sea. The low bias in temperature and high bias in wind speed can impact the prediction of chemical species mixing ratios. For example, the chemical

reactions likely will proceed at a slightly lower rate (because of their dependence on temperature) resulting in formation of products further away from the source. Additionally, biogenic emissions may be underpredicted, since these emissions increase with increasing temperatures and a low bias in temperature can lead to lower emissions.

WRF reasonably predicts the precipitation pattern in March (Fig. 6a–c) when compared to TRMM and GPCC data. Low precipitation is observed over the coast of Burma, the northern part of the South China Sea, and the tip of the Indochina peninsula, and high precipitation is predicted near the equator over the oceans, Malaysian peninsula, and Indonesia. However, the WRF results overestimate precipitation near the equator by 10 to 100 mm for March. In December (Fig. 6d–f), WRF also overpredicts the magnitude of precipitation over the water, but shows reasonable agreement north of 10° N especially over land. The precipitation in this region is dominated by rain from convection, which is controlled by mesoscale processes. The WRF simulations presented here have a 36 km horizontal resolution, and at this resolution, the model relies on a cumulus parameterization to produce the rain. Due to the coarse model resolution for a region with plenty of tropical convection, a situation which is notoriously difficult to represent in models, the poor prediction of precipitation near the equator is not unexpected. Koo and Hong (2010) also found oceanic convection to be overpredicted by the WRF model. However, over land, where the chemical predictions of this study are evaluated, the WRF precipitation has better agreement with observations. As a consequence of the higher precipitation predicted by WRF, WRF-chem may overpredict the removal of soluble trace gases (e.g. nitric acid), thereby affecting the photochemistry in the region.

5.2 Evaluation of chemistry

5.2.1 Ensemble surface means and variations

To show the distribution of the monthly-mean surface mixing ratios for CO, O₃, and NO_x in March and December, the WRF-Chem results from all five simulations (with different

Effect of different emission inventories

T. Amnuaylojaroen et al.

Title Page

Abstract

Introduction

Conclusions

References

Tables

Figures

◀

▶

◀

▶

Back

Close

Full Screen / Esc

Printer-friendly Version

Interactive Discussion



Effect of different emission inventories

T. Amnuaylojaroen et al.

Title Page

Abstract

Introduction

Conclusions

References

Tables

Figures

◀

▶

◀

▶

Back

Close

Full Screen / Esc

Printer-friendly Version

Interactive Discussion



emissions inventories) have been averaged giving an ensemble mean (Fig. 7). In general, surface-level CO and NO_x mixing ratios have highest values over the land regions and lowest values over the ocean near the equator. The influence of biomass burning emissions is evident for all three species over the northern region of the Indochina peninsula during March compared to December. CO mixing ratios are > 100 ppbv over most of the domain with values over 500 ppbv near Bangladesh and southern China for both months and in Burma and northern Thailand for March. Monthly-averaged ozone mixing ratios, which reach 70–90 ppbv, are largest during March over the regions where biomass burning is occurring and downwind of these emissions. With a shorter lifetime, high NO_x mixing ratios of 4–30 ppbv are confined to regions close to the NO_x sources.

The variation in the predicted monthly-averaged surface mixing ratios of CO, O₃, and NO_x across the five simulations is highlighted in Fig. 8. CO mixing ratios vary across simulations by < 20 %, but variations of ~ 30–60 % are found near Bangladesh and Indonesia for both March and December. Ozone mixing ratios have up to 30 % variation near the tip of the Malaysian peninsula and near Indonesia, but have much smaller variability elsewhere. Mixing ratios of NO_x have the most variation among the simulations. The 70–100 % variations for NO_x, especially over the South China Sea, are from the differences in ship emissions from each inventory. There are also high NO_x variations in several cities as seen by the locally high values in Fig. 8e and f.

5.2.2 CO evaluation

The 6-hourly daytime (00:00, 06:00, 12:00 UTC) CO mixing ratios from WRF-Chem with each of the five inventories are compared to observations from the six ground-site measurements: Chiang Mai (CM), Khonkaen (KK), Nonthaburi (NTB), Chonburi (CB) and Suratthani (SRT) (Fig. 5g). These sites are located in urban environments with background conditions ranging from high biomass burning in northern Thailand to more marine conditions in southern Thailand. For March when biomass burning emissions are a large source of CO, the WRF-Chem simulations agree well with the monthly-mean mixing ratio for Chiang-Mai in northwest Thailand and Chonburi in southeast

Effect of different emission inventories

T. Amnuaylojaroen et al.

Title Page

Abstract

Introduction

Conclusions

References

Tables

Figures

◀

▶

◀

▶

Back

Close

Full Screen / Esc

Printer-friendly Version

Interactive Discussion



sions. One issue with coarse resolution modeling of biomass burning emissions is that multiple fires in one model grid cell are aggregated into a single, bigger fire area. This aggregated information is used by the plumerise model in WRF-Chem, which may erroneously apply too much thermal buoyancy associated with the fires, resulting in emissions placed too high above the ground. For example, WRF-Chem results without the plumerise feature of biomass burning emissions, as illustrated by the March monthly-averaged CO vertical profiles at Yangon, Burma (Fig. 16), show that injection into the lowest model level gives vertical profiles more consistent with MOZART results, which injects fire emissions into the lowest model level. Thus, in the simulations with the plumerise feature, ozone precursor species (NMVOCs and NO_x) may be placed in an environment where ozone production is more productive than if the precursors were placed near the surface. While these results indicate a substantial difference in CO mixing ratios in the lowest 500 hPa of the atmosphere, observations of CO vertical profiles are needed to help evaluate the model predictions. In addition, trash burning emissions are not included in this study, yet have been shown to have a significant contribution to the air quality (Hodzic et al., 2012). In reality, Southeast Asia has complex emission sources that not only include biomass burning and anthropogenic activities, but also biofuel and trash burning. To improve simulations of carbon monoxide in the future, these other emissions should be included. The underprediction of NO₂ in all the WRF-chem simulations suggests that the anthropogenic NO_x emissions are underestimated over the Southeast Asia. These errors in anthropogenic emission estimates are likely due to uncertainties in including all the CO or NO_x sources from the different emission sectors and estimating the emission factors from the different sources.

The variation in NO shipping emissions, as seen by the comparison of the simulation using only the SEAC4RS emissions without shipping emissions with the simulation using MACCity-SEAC4RS emissions, does produce substantial variation among model predictions of NO₂ (Fig. 14) and O₃ (Fig. 13). Therefore, it is important to include the shipping sector as part of the emissions inventory.

Effect of different emission inventories

T. Amnuaylojaroen et al.

Title Page

Abstract

Introduction

Conclusions

References

Tables

Figures

◀

▶

◀

▶

Back

Close

Full Screen / Esc

Printer-friendly Version

Interactive Discussion



This paper did not include the REAS emissions inventory. For Southeast Asia the REAS v2.1 CO emissions are similar to the TRACE-P (Streets et al., 2003) and INTEX-B (Zhang et al., 2009) emission inventories for years 2000 and 2006, respectively. The REAS v2.1 NO_x emissions are also similar to the TRACE-P emissions inventory for 2000, but are lower than the INTEX-B inventory for year 2006 (Kurakawa et al., 2013). We would then expect the REAS v2.1 inventory to produce similar results for CO surface mixing ratios as the INTEX-B emissions inventory did, but have lower NO_x mixing ratios, if the year 2006 REAS inventory is used. The 2008 REAS v2.1 emissions are 10–20 % greater than their 2006 emissions. These increased emissions would likely give results for CO and O₃ surface mixing ratios that are < 10 % greater than the mixing ratios simulated in this study. To confirm this, additional WRF-Chem simulations should be done with the REAS emissions inventory.

The goal of this paper is to examine the differences in predicted CO and O₃ mixing ratios at the surface when different anthropogenic emission inventories are used. Table 6 lists monthly-average ozone and carbon monoxide mixing ratios on land for March and December for all of the simulation cases. During the biomass-burning season (March), the average CO differs by less than 5 ppbv (< 1 % difference) among the different emission inventories, while average ozone ranges from 146 to 160 ppbv (9 % difference) among the different emission inventories. In December when anthropogenic emissions are greater than biomass burning emissions, the differences in average CO and O₃ among the different emission inventories is very small (2 ppbv for CO and 7 ppbv for O₃). These small variations, which are also seen in the mean bias calculations for the ground-based sites (Tables 3 and 5), suggest that the choice of the emission inventory does not have a substantial effect on CO and O₃ surface concentrations, despite the different emission inventories having a ~ 30 % variation for CO and 10 % variation for NO emissions.

By comparing the March average mixing ratios to the December average mixing ratios (Table 6), the importance of biomass burning emissions on ozone and carbon monoxide variability is revealed. In March, CO is 16 % greater than CO in December

for all simulations except that with RETRO emissions. The average O₃ in March is ~ 30 % greater than average O₃ in December. These differences are much greater than those induced by the anthropogenic emissions in Southeast Asia. Thus, biomass burning emissions produce more variability in WRF-Chem simulation results than the different anthropogenic emission inventories.

7 Conclusion

This study presents WRF-Chem results to show the variability of emissions on surface ozone and carbon monoxide mixing ratios in Southeast Asia. The predicted meteorological fields are evaluated with reanalysis output (MERRA), satellite data (TRMM) and ground-based observations (GPCC) for 2 m temperature, wind, and precipitation. Surface CO and O₃ mixing ratios are compared to ground-based monitoring observations in Thailand. Surface CO is also compared to MOPITT satellite data. Ozone vertical profiles are compared with SHADOZ ozonesonde data, and the NO₂ tropospheric column is evaluated with OMI satellite data.

In general, the temperature and winds showed good agreement with MERRA output, although there was a slight underestimate of temperature and slight overestimate of wind speed. Precipitation was reasonably predicted for regions north of 10° N in comparison to TRMM and GPCC data, but was overestimated near the equator. By using a grid spacing of 36 km, the precipitation was generated mostly by the cumulus parameterization in the model resulting in a less reliable prediction of rain and convective mass fluxes between the boundary layer and mid- to upper troposphere. Surface O₃ mixing ratios were generally higher than observations and surface CO mixing ratios were lower than observations. Although the emission inventories were for years other than that simulated here, the differences in surface O₃ and CO mixing ratios among the simulations with different inventories were small. Thus, the model biases are likely not the result of the emission inventory trends but more likely caused by the omission of sources such as trash burning and biofuel use and uncertainties not fully captured in

Effect of different emission inventories

T. Amnuaylojaroen et al.

Title Page

Abstract

Introduction

Conclusions

References

Tables

Figures

◀

▶

◀

▶

Back

Close

Full Screen / Esc

Printer-friendly Version

Interactive Discussion



Effect of different emission inventories

T. Amnuaylojaroen et al.

Title Page

Abstract

Introduction

Conclusions

References

Tables

Figures

◀

▶

◀

▶

Back

Close

Full Screen / Esc

Printer-friendly Version

Interactive Discussion



the current emission inventories. Further study of the role of different emission sectors on CO and O₃ can help elucidate where the major weaknesses are in the emission inventories. In addition, analysis of the contribution of CO, NO_x, O₃, and VOCs from outside the Southeast Asia region on the region's air quality should be compared with the contribution of the local emissions.

Simulations using different anthropogenic emissions created only a slight variability of O₃ and CO mixing ratios, while biomass burning emissions added more variability. The different anthropogenic emissions have up to 30 % difference in CO emissions but only a small change of O₃ and CO mixing ratios of ~ 4.5 % and ~ 8 %, respectively, among the simulations. By comparing March (when biomass burning is at its peak) surface mixing ratios to December values, it is found that biomass burning emissions substantially increase both ozone and carbon monoxide mixing ratios by ~ 30 % and ~ 16 %.

Southeast Asia is a region with complex terrain and emission sources at small scales. Thus, one important test to improve the regional-scale simulations of air quality in Southeast Asia would be to use model grid spacing of the order of 10 km or less. A higher grid resolution should also reduce errors in the injection height of biomass burning emissions. However, a high-resolution simulation needs emission inventories at equally high resolution. Inclusion of other types of emissions, e.g. trash emissions, in the current inventories could also improve the representation of the atmospheric chemistry in Southeast Asia. Lastly, particulate matter (aerosols) was not addressed in this study. Not only should their contribution to air quality be evaluated, but their impact on gas-phase photochemistry should be addressed.

Acknowledgements. The authors would like to thank the National Center for Atmospheric Research (NCAR) Advanced Study Program (ASP) for the scholarship to visit the Atmospheric Chemistry Division (ACD), the Center for Environmental Health, Toxicology and Management of Chemical, Chiang Mai University, Faculty of Science, Chiang Mai, Thailand for Ph.D. scholarship, and the Graduate School Chiang Mai University for partial support. The study was partially supported by NSF CHEM award 1049058. We are thankful for the Thai Pollution Control Department (PCD) providing their O₃ and CO observation data. We also acknowledge the Global

Effect of different emission inventories

T. Amnuaylojaroen et al.

Modeling and Assimilation Office (GMAO) and the GES DISC for the dissemination of MERRA, the NASA Goddard Space Flight Center for providing SHADOZ data, and the NASA Langley Research Center Atmospheric Science Data Center for providing MOPITT data. Analyses and visualizations used in this paper were produced with the Giovanni online data system, developed and maintained by the NASA GES DISC. We acknowledge Gabriele Pfister and Sachin Ghude for their assistance with WRF-Chem simulations. The comments from Christine Wiedinmyer and Rajesh Kumar are greatly appreciated. NCAR is operated by the University Corporation for Atmospheric Research (UCAR) under sponsorship of the National Science Foundation.

References

- Adhikary, B., Carmichael, G. R., Tang, Y., Leung, L. R., Qian, Y., Schauer, J. J., Stone, E. A., Ramanathan, V., and Ramana, M. V.: Characterization of South Asian Aerosols during the ABC-Post Monsoon Experiment (ABC-APMEX): a regional-scale modeling analysis, *J. Geophys. Res.*, 112, D22S22, doi:10.1029/2006JD008143, 2007.
- Akimoto, H. and Narita, H.: Distribution of SO₂, NO_x, and CO₂ emissions from fuel combustion and industrial activities in Asia with 1° × 1° resolution, *Atmos. Environ.*, 28, 213–225, 1994.
- Amnuaylojaroen, T. and Kreasuwun, J.: Investigation of fine and coarse particulate matter from burning areas in Chiang Mai, Thailand using the WRF/CALPUFF, *Chiang Mai, J. Sci.*, 39, 1–16, 2012.
- Boersma, K. F., Jacob, D. J., Eskes, H. J., Pinder, R. W., Wand, J., and Vander A, R. J.: Intercomparison of SCIAMACHY and OMI tropospheric NO₂ columns: observing the diurnal evolution of chemistry and emissions from space, *J. Geophys. Res.*, 113, D16S26, doi:10.1029/2007JD008816, 2008.
- Boersma, K. F., Jacob, D. J., Trainic, M., Rudich, Y., DeSmedt, I., Dirksen, R., and Eskes, H. J.: Validation of urban NO₂ concentrations and their diurnal and seasonal variations observed from the SCIAMACHY and OMI sensors using in situ surface measurements in Israeli cities, *Atmos. Chem. Phys.*, 9, 3867–3879, doi:10.5194/acp-9-3867-2009, 2009.
- Bucsel, E. J., Celarier, E. A., Wening, M. O., Gleason, J. F., Veefkind, J. P., Boersma, K. F., and Brinksma, E. J.: Algorithm for NO₂ vertical column retrieval from the Ozone Monitoring Instrument, *IEEE T. Geosci. Remote*, 44, 1245–1258, 2006.

Title Page

Abstract

Introduction

Conclusions

References

Tables

Figures

◀

▶

◀

▶

Back

Close

Full Screen / Esc

Printer-friendly Version

Interactive Discussion



Effect of different emission inventories

T. Amnuaylojaroen et al.

Title Page

Abstract

Introduction

Conclusions

References

Tables

Figures

◀

▶

◀

▶

Back

Close

Full Screen / Esc

Printer-friendly Version

Interactive Discussion



Chen, F. and Dudhia, J.: Coupling an advanced land-surface/hydrology model with the Penn State/NCAR MM5 modeling system, Part 1: Model description and implementation, *Mon. Weather. Rev.*, 129, 569–585, 2001.

Chin, M., Rood, R. B., Lin, S.-J., Muller, J. F., and Thompson, A. M.: Atmospheric sulfur cycle in the global model GOCART: model description and global properties, *J. Geophys. Res.*, 105, 24671–24687, 2000.

Chou, M.-D. and Suarez, M. J.: An efficient thermal infrared radiation parameterization for use in general circulation models, NASA Tech. Memo. 104606, 3, 85 pp., NASA/GSFC, Greenbelt, MD, 1994.

Deeter, M. N.: MOPITT (Measurement of Pollution in the Troposphere) Version6 Product User's Guide, available at: http://www2.acd.ucar.edu/sites/default/files/mopitt/v6_users_guide_201309.pdf (last access: 26 March 2014), 2013

Deeter, M. N., Martinez-Alonso, S., Edwards, D. P., Emmons, L. K., Gille, J. C., Worden, H. M., Pittman, J. V., Daube, B. C., and Wofsy, S. C.: Validation of MOPITT version 5 thermal-infrared, near-infrared, and multispectral carbon monoxide profile retrievals for 2000–2011, *J. Geophys. Res.*, 118, 6710–6725, doi:10.1002/jgrd.50272, 2013.

Deng, X., Tie, X., and Zhou, X.: Effects of Southeast Asia biomass burning on aerosols and ozone concentrations over the Pearl River Delta (PRD) region, *Atmos. Environ.*, 42, 8493–8501, doi:10.1016/j.atmosenv.2008.08.013, 2008.

Emmons, L. K., Deeter, M. N., Gille, J. C., Edwards, D. P., Attie, J.-L., Warner, J., Ziskin, D., Francis, G., Khattatov, B., Yudin, V., Lamarque, J. -F., Ho, S. -P., Mao, D., Chen, J. S., Drummond, J., Novelli, P., Sachse, G., Coffey, M., Hannigan, J. W., Gerbig, C., Kawakami, S., Kondo, Y., Takegawa, N., Schlager, H., Baehr, J., and Ziereis, H.: Validation of Measurements of Pollution in the Troposphere (MOPITT) CO retrievals with aircraft in situ profiles, *J. Geophys. Res.*, 109, D03309, doi:10.1029/2003JD004101, 2004.

Emmons, L. K., Pfister, G. G., Edwards, D. P., Gille, J. C., Sachse, G., Blake, D., Wofsy, S., Gerbig, C., Matross, D., and Nedelec, P.: Measurements of Pollution in the Troposphere (MOPITT) validation exercises during summer 2004 field campaigns over North America, *J. Geophys. Res.*, 112, D12S02, doi:10.1029/2006JD007833, 2007.

Emmons, L. K., Edwards, D. P., Deeter, M. N., Gille, J. C., Campos, T., Nédélec, P., Novelli, P., and Sachse, G.: Measurements of Pollution In The Troposphere (MOPITT) validation through 2006, *Atmos. Chem. Phys.*, 9, 1795–1803, doi:10.5194/acp-9-1795-2009, 2009.

Effect of different emission inventories

T. Amnuaylojaroen et al.

Title Page

Abstract

Introduction

Conclusions

References

Tables

Figures

◀

▶

◀

▶

Back

Close

Full Screen / Esc

Printer-friendly Version

Interactive Discussion



- Emmons, L. K., Walters, S., Hess, P. G., Lamarque, J.-F., Pfister, G. G., Fillmore, D., Granier, C., Guenther, A., Kinnison, D., Laepple, t., Orlando, J., Tie, X., Tyndall, G., Wiedinmyer, C., Baughcum, S. L., and Kloser, S.: Description and evaluation of the Model for Ozone and Related chemical Tracers, version 4 (MOZART4), *Geosci. Model. Dev.*, 3, 43–67, 2010.
- 5 Fast, J. D., Gustafson Jr, W. I., Easter, R. C., Zaveri, R. A., Barnard, J. C., Chapman, E. G., and Grell, G. A.: Evolution of ozone, particulates, and aerosol direct forcing in an urban area using a new fully-coupled meteorology, chemistry, and aerosol model, *J. Geophys. Res.*, 111, D21305, doi:10.1029/2005JD006721, 2006.
- Geng, F., Tie, X., Guenther, A., Li, G., Cao, J., and Harley, P.: Effect of isoprene emissions from major forests on ozone formation in the city of Shanghai, China, *Atmos. Chem. Phys.*, 11, 10449–10459, doi:10.5194/acp-11-10449-2011, 2011.
- 10 Ghude, S. D., Pfister, G. G., Jena, C. K., Van der A, R. J., Emmons, L. K., and Kumar, R.: Satellite constraints of nitrogen oxide (NO_x) emissions from India based on OMI observations and WRF-Chem simulations, *Geophys. Res. Lett.*, 40, 1–6, doi:10.1029/2012GL053926, 2013.
- 15 Granier, C., Bessagnet, B., Bond, T., Angiola, A. D., Van Der Gon, H. D., Frost, G. J., Heil, A., Kaiser, J. W., Kinne, S., Klimont, Z., Kloster, S., Lamarque, J. -F., Liousse, C., Masui, T., Meleux, F., Mieville, A., Ohara, T., Raut, J.-C., Riahi, K., Schultz, M. G., Smith, S. J., Thompson, A., Aardenne, J. V., Vander Werf, G. R., and Van Vuuren, D. P.: Evolution of anthropogenic and biomass burning emission of air pollutants at global and regional scales during the 1980–2010 period, *Climatic Change*, 109, 163–190, 2011.
- 20 Grell, G. A. and Devenyi, D.: A generalized approach to parameterizing convection combining ensemble and data assimilation techniques, *Geophys. Res. Lett.*, 29, 1693, doi:10.1029/2002GL015311, 2002.
- Grell, G. A., Peckham, S. E., Schmitz, R., McKeen, S. A., Frost, G., Skamarock, W. C., and Eder, B.: Fully coupled “online” chemistry within the WRF model, *Atmos. Environ.*, 29, 6957–6975, 2005.
- 25 Guenther, A., Karl, T., Harley, P., Wiedinmyer, C., Palmer, P. I., and Geron, C.: Estimates of global terrestrial isoprene emissions using MEGAN (Model of Emissions of Gases and Aerosols from Nature), *Atmos. Chem. Phys.*, 6, 3181–3210, doi:10.5194/acp-6-3181-2006, 2006.
- 30 Han, Z., Sakurai, T., Ueda, H., Matsuda, K., Hozumi, Y., Carmichael, G. R., Streets, D. G., Park, S. U., Fung, C., Chang, A., Kajino, M., Thongboonchoo, N., Engardt, M., Bennet, C., Hayami, H., Sartelet, K., Holloway, T., Wang, Z., and Amann, M.: Model intercomparison and

Effect of different emission inventories

T. Amnuaylojaroen et al.

Title Page

Abstract

Introduction

Conclusions

References

Tables

Figures

◀

▶

◀

▶

Back

Close

Full Screen / Esc

Printer-friendly Version

Interactive Discussion



evaluation of ozone and relevant species – MICS-Asia phase II study, *Atmos. Environ.*, 42, 3491–3509, 2008.

Hodzic, A., Wiedinmyer, C., Salcedo, D., and Jimenez, J. L.: Impact of trash burning on air quality in Mexico City, *Environ. Sci. Technol.*, 46, 4950–4957, doi:10.1021/es203954r, 2012.

5 Hollingsworth, A., Engelen, R. J., Textor, C., Benedetti, A., Boucher, O., Chevallier, F., De-
thof, A., Elbern, H., Eskes, H., Flemming, J., Granier, C., Morcrette, J. J., Rayner, P.,
Peuch, V.-H., Rouil, L., Schultz, M., and Simmons, A. J.: Toward a monitoring and fore-
casting system for atmospheric composition: the GEMS project, *B. Am. Meteorol. Soc.*, 89,
1147–1164, doi:10.1175/2008BAMS2355.1, 2008.

10 Huffman, G. J. and Bolvin, D. T.: TRMM and Other Data Precipitation Data Set Document,
available at: ftp://precip.gsfc.nasa.gov/pub/trmmdocs/3B42_3B43_doc.pdf (last access: 26
March 2014), 2012

Huffman, G. J., Adler, R. F., Arkin, P., Chang, A., Ferraro, R., Gruber, A., Janowiak, J., Mc-
Nab, A., Rudolph, B., and Schneide, U.: The Global Precipitation Climatology Project (GPCP)
15 combined precipitation dataset, *B. Am. Meteorol. Soc.*, 78, 5–20, 1997.

Janjic, Z. I.: Nonsingular Implementation of the Mellor–Yamada Level 2.5 Scheme in the NCEP
Meso model, National Oceanic and Atmospheric Administration Science Center, Camp
Springs, MD, NCEP Office Note, No. 437, 61, 2002.

20 Koo, M.-S. and Hong, S.-Y.: Diurnal variations of simulated precipitation over East Asia in two
regional climate models, *J. Geophys. Res.*, 115, D05105, doi:10.1029/2009JD012574, 2010.

Kramer, L. J., Leigh, R. J., Remedios, J. J., and Monks, P. S.: Comparison of OMI and ground-
based in situ and MAX-DOAS measurements of tropospheric nitrogen dioxide in an urban
area, *J. Geophys. Res.*, 113, D16S39, doi:10.1029/2007jd009168, 2008.

25 Kumar, R., Naja, M., Pfister, G. G., Barth, M. C., and Brasseur, G. P.: Source attribution of
carbon monoxide in India and surrounding regions during wintertime, *J. Geophys. Res.*, 118,
1981–1995, doi:10.1002/jgrd.50134, 2013.

Kurokawa, J., Ohara, T., Morikawa, T., Hanayama, S., Janssens-Maenhout, G., Fukui, T.,
Kawashima, K., and Akimoto, H.: Emissions of air pollutants and greenhouse gases over
Asian regions during 2000–2008: Regional Emission inventory in ASia (REAS) version 2,
30 *Atmos. Chem. Phys.*, 13, 11019–11058, doi:10.5194/acp-13-11019-2013, 2013.

Lamarque, J.-F., Bond, T. C., Eyring, V., Granier, C., Heil, A., Klimont, Z., Lee, D., Liousse, C.,
Mieville, A., Owen, B., Schultz, M. G., Shindell, D., Smith, S. J., Stehfest, E., Van Aar-
denne, J., Cooper, O. R., Kainuma, M., Mahowald, N., McConnell, J. R., Naik, V., Riahi, K.,

Effect of different emission inventories

T. Amnuaylojaroen et al.

Title Page

Abstract

Introduction

Conclusions

References

Tables

Figures

◀

▶

◀

▶

Back

Close

Full Screen / Esc

Printer-friendly Version

Interactive Discussion



and van Vuuren, D. P.: Historical (1850–2000) gridded anthropogenic and biomass burning emissions of reactive gases and aerosols: methodology and application, *Atmos. Chem. Phys.*, 10, 7017–7039, doi:10.5194/acp-10-7017-2010, 2010.

Liu, C.-H., Yeh, M. T., and Paul, S.: Effect of anthropogenic emissions in East Asia on regional ozone levels during spring cold continental outbreaks near Taiwan: a case study, *Environ. Modell. Softw.*, 23, 579–591, 2008.

Lu, Z. and Streets, D. G.: The Southeast Asia Composition, Cloud, Climate Coupling Regional Study Emission Inventory, available at: <http://bio.cgrrer.uiowa.edu/SEAC4RS/emission.html> (last access: 26 March 2014), 2012.

Mlawer, E. J., Taubman, S. J., Brown, P. D., Iacono, M. J., and Clough, S. A.: Radiative transfer for inhomogeneous atmosphere: RRTM, a validated correlated-k model for the longwave, *J. Geophys. Res.*, 102, 16663–16682, 1997.

Neu, J. L. and Prather, M. J.: Toward a more physical representation of precipitation scavenging in global chemistry models: cloud overlap and ice physics and their impact on tropospheric ozone, *Atmos. Chem. Phys.*, 12, 3289–3310, doi:10.5194/acp-12-3289-2012, 2012.

Ohara, T., Akimoto, H., Kurokawa, J., Horii, N., Yamaji, K., Yan, X., and Hayasaka, T.: An Asian emission inventory of anthropogenic emission sources for the period 1980–2020, *Atmos. Chem. Phys.*, 7, 4419–4444, doi:10.5194/acp-7-4419-2007, 2007.

Olivier, J. G. J., Van Aardenne, J. A., Dentener, F., Ganzeveld, L., and Peters, J. A. H. W.: Recent trends in global greenhouse gas emissions: regional trends and spatial distribution of key sources, *Environ. Sci.*, 2, 81–99, doi:10.1080/15693430500400345, 2005.

Rienecker, M. M., Suarez, M. J., Gelaro, R., Todling, R., Bacmeister, J., Liu, E., Bosilovich, M. G., Schubert, S. D., Takacs, L., Kim, G.-K., Bloom, S., Chen, J., Collins, D., Conaty, A., Da Silva, A., Gu, W., Joiner, J., Koster, R. D., Lucchesi, R., Molod, A., Owens, T., Pawson, S., Pegion, P., Redder, C. R., Reichle, R., Robertson, F. R., Ruddick, A. G., Sienkiewicz, M., and Woollen, J.: MERRA – NASA’s Modern-Era Retrospective Analysis for Research and Applications, *J. Climate*, 24, 3624–3648, doi:10.1175/JCLI-D-11-00015.1, 2011.

Rudolf, B. and Schneider, U.: Calculation of Gridded Precipitation Data for the Global Land-Surface using in-situ Gauge Observations, Proceedings of the 2nd Workshop of the International Precipitation Working Group IPWG, Monterey, 25–28 October 2004, EUMETSAT, 231–247, 2005.

Effect of different emission inventories

T. Amnuaylojaroen et al.

Title Page

Abstract

Introduction

Conclusions

References

Tables

Figures

◀

▶

◀

▶

Back

Close

Full Screen / Esc

Printer-friendly Version

Interactive Discussion



Sandu, A. and Sander, R.: Technical note: Simulating chemical systems in Fortran90 and Matlab with the Kinetic PreProcessor KPP-2.1, *Atmos. Chem. Phys.*, 6, 187–195, doi:10.5194/acp-6-187-2006, 2006.

Schneider, U., Becker, A., and Meyer-Christofer, A.: Global Precipitation Analysis Products of the GPCC, available at: ftp://ftp-anon.dwd.de/pub/data/gpcc/PDF/GPCC_intro_products_2008.pdf (last access: 27 March 2014), 2011a.

Schneider, U., Becker, A., Finger, P., Meyer-Christoffer, A., Rudolf, B., Ziese, M.: GPCC Full Data Reanalysis Version 6.0 at 1.0deg: Monthly Land-Surface Precipitation from Rain-Gauges built on GTS-based and Historic Data, doi:10.5676/DWD_GPCC/FD_M_V6_100, 2011b.

Schultz, M., Rast, S., van het Bolscher, M., Pulles, T., Pereira, J., Spessa, A., Dalsøren, S., van Noije, T., and Szopa, S.: REanalysis of the TROpospheric chemical composition over the past 40 years, a long-term global modeling study of tropospheric chemistry funded under the 5th EU framework programme, Tech. rep., EU-Contract No. EVK2-CT-2002-00170, available at: http://retro.enes.org/reports/D1-6_final.pdf (last access: 27 March 2014), 2007.

Skamarock, W. C., Klemp, J. B., Duhia, J., Gill, D. O., Barker, D. M., Duda, M. G., Huang, X.-Y., Wang, W., and Powers, J. G.: A Description of the Advanced Research WRF Version 3, NCAR Technical note, National Center for Atmospheric Research, Boulder, CO, USA, 2008.

Shepard, D.: A two-dimensional interpolation function for irregularly spaced data, in *Proceedings of the 1968 23rd ACM National Conference*, ACM, New York, NY, USA, 517–524, 1968.

Stauffer, D. R. and Seaman, N. L.: Use of four-dimensional data assimilation in a limited area mesoscale model, Part 1: Experiments with synoptic-scale data, *Mon. Weather. Rev.*, 118, 1250–1277, 1990.

Streets, D. G., Bond, T. C., Carmichael, G. R., Fernandes, S. D., Fu, Q., He, D., Klimont, Z., Nelson, S. M., Tsai, N. Y., Wang, M. Q., Woo, J.-H., and Yarber, K. F.: An inventory of gaseous and primary aerosol emissions in Asia in the year 2000, *J. Geophys. Res.*, 108, 8809, doi:10.1029/2002JD003093, 2003.

Tanimoto, H., Ohara, T., and Uno, I.: Asian anthropogenic emissions and decadal trends in springtime tropospheric ozone over Japan: 1998–2007, *Geophys. Res. Lett.*, 36, L23802, doi:10.1029/2009GL041382, 2009.

Thompson, A. M., Miller, S. K., Tilmes, S., Kollonige, D. W., Witte, J. C., Oltmans, S. J., Johnson, B. J., Fujiwara, M., Schmidlin, F. J., Coetsee, G. J. R., Komala, N., Maata, M., Mohamad, M., Nguyo, J., Mutai, C., Ogino, S. -Y., Da Silva, R. F., Paes Leme, N. M., Posny, F.,

Effect of different emission inventories

T. Amnuaylojaroen et al.

Title Page

Abstract

Introduction

Conclusions

References

Tables

Figures

◀

▶

◀

▶

Back

Close

Full Screen / Esc

Printer-friendly Version

Interactive Discussion



Scheele, R., Selkirk, H. B., Shiotani, M., Stubi, R., Levrat, G., Calpini, B., Thouret, V., Tsuruta, H., Canossa, J. V., Vomel, H., Yonemura, S., Diaz, J. A., Tan Thanh, N. T., and Ha, T.: Southern Hemisphere Additional Ozonesondes (SHADOZ) ozone climatology (2005–2009): Tropospheric and tropical tropopause layer (TTL) profiles with comparisons to OMI-based ozone products, *J. Geophys. Res.*, 117, D23301, doi:10.1029/2011JD016911, 2012.

Thompson, G., Rasmussen, R. M., and Manning, K.: Explicit forecasts of winter precipitation using an improved bulk microphysics scheme, Part 1: Description and sensitivity analysis, *Mon. Weather. Rev.*, 132, 519–542, 2004.

Tie, X., Madronich, S., Walters, S., Zhang, R., Rasch, P., and Collins, W.: Effects of clouds on photolysis and oxidants in the troposphere, *J. Geophys. Res.*, 108, 4642, doi:10.1029/2003JD003659, 2003.

Van Vuuren, D. P., Edmonds, J., Kainuma, M., Riahi, K., Thomson, A., Hibbard, K., Hurtt, G. C., Kram, T., Krey, V., and Lamarque, J.-F.: The representative concentration pathways: an overview, *Climatic Change*, 109, 5–31, 2011.

Wang, H., Skamarock, W. C., and Feingold, G.: Evaluation of scalar advection schemes in the advanced research WRF model using large-eddy simulations of aerosol–cloud interactions, *Mon. Weather. Rev.*, 137, 2547–2558, 2009.

Wang, X., Carmichael, G. R., Chen, D., Tang, Y., and Wang, T.: Impacts of different emission sources on air quality during March 2001 in the Pearl River Delta (PRD) region, *Atmos. Environ.*, 39, 5227–5241, doi:10.1016/j.atmosenv.2005.04.035, 2005.

Wang, Y., Zhang, Y., Hao, J., and Luo, M.: Seasonal and spatial variability of surface ozone over China: contributions from background and domestic pollution, *Atmos. Chem. Phys.*, 11, 3511–3525, doi:10.5194/acp-11-3511-2011, 2011.

Wesley, M. L.: Parameterization of surface resistance to gaseous dry deposition in regional numerical models, *Atmos. Environ.*, 16, 1293–1304, 1989.

Wiedinmyer, C., Akagi, S. K., Yokelson, R. J., Emmons, L. K., Al-Saadi, J. A., Orlando, J. J., and Soja, A. J.: The Fire INventory from NCAR (FINN): a high resolution global model to estimate the emissions from open burning, *Geosci. Model Dev.*, 4, 625–641, doi:10.5194/gmd-4-625-2011, 2011.

Willmott, C. J., Rowe, C. M., Philpot, W. D.: Small scale climate maps: a sensitivity analysis of some common assumption associated with grid point interpolation and contouring, *Am. Cartographer*, 12, 5–16, 1985.

- Zhang, Q., Streets, D. G., Carmichael, G. R., He, K. B., Huo, H., Kannari, A., Klimont, Z., Park, I. S., Reddy, S., Fu, J. S., Chen, D., Duan, L., Lei, Y., Wang, L. T., and Yao, Z. L.: Asian emissions in 2006 for the NASA INTEX-B mission, *Atmos. Chem. Phys.*, 9, 5131–5153, doi:10.5194/acp-9-5131-2009, 2009.
- 5 Zhou, Y., Brunner, D., Boersma, K. F., Dirksen, R., and Wang, P.: An improved tropospheric NO₂ retrieval for OMI observations in the vicinity of mountainous terrain, *Atmos. Meas. Tech.*, 2, 401–416, doi:10.5194/amt-2-401-2009, 2009.

Effect of different emission inventories

T. Amnuaylojaroen et al.

Title Page

Abstract

Introduction

Conclusions

References

Tables

Figures

◀

▶

◀

▶

Back

Close

Full Screen / Esc

Printer-friendly Version

Interactive Discussion



Effect of different emission inventories

T. Amnuaylojaroen et al.

Table 2. Monthly-average correlation coefficients (r) of daytime (00:00, 06:00, 12:00 UTC) carbon monoxide.

Emission Inventories	CM		KK		SRB		NTB		CBR		SRT	
	Mar	Dec										
RETRO	0.49	0.13	0.35	0.10	0.27	0.15	0.40	0.31	0.48	0.15	0.52	0.03
INTEX-B	0.51	0.14	0.42	0.20	0.17	0.17	0.33	0.38	0.44	0.17	0.58	0.03
MACCity	0.50	0.14	0.45	0.10	0.11	0.19	0.26	0.33	0.43	0.19	0.55	0.003
SEAC4RS	0.48	0.15	0.42	0.04	0.09	0.18	0.21	0.33	0.42	0.18	0.52	0.01
MACCity/ SEAC4RS	0.48	0.15	0.41	0.07	0.12	0.14	0.26	0.33	0.44	0.14	0.54	0.004

[Title Page](#)
[Abstract](#)
[Introduction](#)
[Conclusions](#)
[References](#)
[Tables](#)
[Figures](#)
[◀](#)
[▶](#)
[◀](#)
[▶](#)
[Back](#)
[Close](#)
[Full Screen / Esc](#)
[Printer-friendly Version](#)
[Interactive Discussion](#)


Effect of different emission inventories

T. Amnuaylojaroen et al.

Table 3. Monthly-average biases of daytime (00:00, 06:00, 12:00 UTC) carbon monoxide.

Emission Inventories	CM		KK		SRB		NTB		CBR		SRT	
	Mar	Dec	Mar	Dec	Mar	Dec	Mar	Dec	Mar	Dec	Mar	Dec
RETRO	-104	-147	-396	-581	-219	-314	-721	-770	-253	23	-267	-89
INTEX-B	-16	-114	-316	-529	-150	-283	-662	-747	-203	46	-234	-109
MACCity	-18	-112	-292	-530	-116	-263	-636	-733	-195	60	-238	-112
SEAC4RS	-22	-107	-324	-548	-129	-267	-645	-734	-197	58	-234	-120
MACCity/ SEAC4RS	-47	-157	-35	-601	-165	-328	-674	-785	-218	10	-243	-93

[Title Page](#)
[Abstract](#)
[Introduction](#)
[Conclusions](#)
[References](#)
[Tables](#)
[Figures](#)
[◀](#)
[▶](#)
[◀](#)
[▶](#)
[Back](#)
[Close](#)
[Full Screen / Esc](#)
[Printer-friendly Version](#)
[Interactive Discussion](#)


Effect of different emission inventories

T. Amnuaylojaroen et al.

Table 5. Monthly-average biases of daytime (00:00, 06:00, 12:00 UTC) ozone.

Emission Inventories	CM		KK		SRB		NTB		CBR		SRT	
	Mar	Dec										
	RETRO	36.48	8.28	23.83	19.36	7.77	13.58	12.15	3.07	17.82	6.96	9.52
INTEX-B	37.76	4.05	32.62	18.26	15.31	12.42	18.54	2.67	23.64	5.58	14.57	29.56
MACCity	39.67	6.19	30.24	15.68	14.62	8.69	18.53	-1.34	24.88	3.04	15.76	30.36
SEAC4RS	38.53	3.75	31.45	20.14	17.29	13.98	27.90	4.61	24.38	6.33	11.26	29.15
MACCity/ SEAC4RS	39.72	5.31	32.45	19.92	16.59	13.37	18.19	-0.25	24.95	5.52	15.38	32.22

[Title Page](#)
[Abstract](#)
[Introduction](#)
[Conclusions](#)
[References](#)
[Tables](#)
[Figures](#)
[◀](#)
[▶](#)
[◀](#)
[▶](#)
[Back](#)
[Close](#)
[Full Screen / Esc](#)
[Printer-friendly Version](#)
[Interactive Discussion](#)


Effect of different emission inventories

T. Amnuaylojaroen et al.

Table 6. Monthly-average surface ozone and carbon monoxide mixing ratios at land-based grid points in Southeast Asia.

Emission Inventories	CO (ppb)		O ₃ (ppb)	
	Mar	Dec	Mar	Dec
RETRO	571	596	146	122
INTEX-B	575	497	156	119
MACCity	574	495	160	122
SEAC4RS	574	494	159	122
MACCity/SEAC4RS	575	495	154	115

[Title Page](#)
[Abstract](#)
[Introduction](#)
[Conclusions](#)
[References](#)
[Tables](#)
[Figures](#)
[◀](#)
[▶](#)
[◀](#)
[▶](#)
[Back](#)
[Close](#)
[Full Screen / Esc](#)
[Printer-friendly Version](#)
[Interactive Discussion](#)


Effect of different emission inventories

T. Amnuaylojaroen et al.

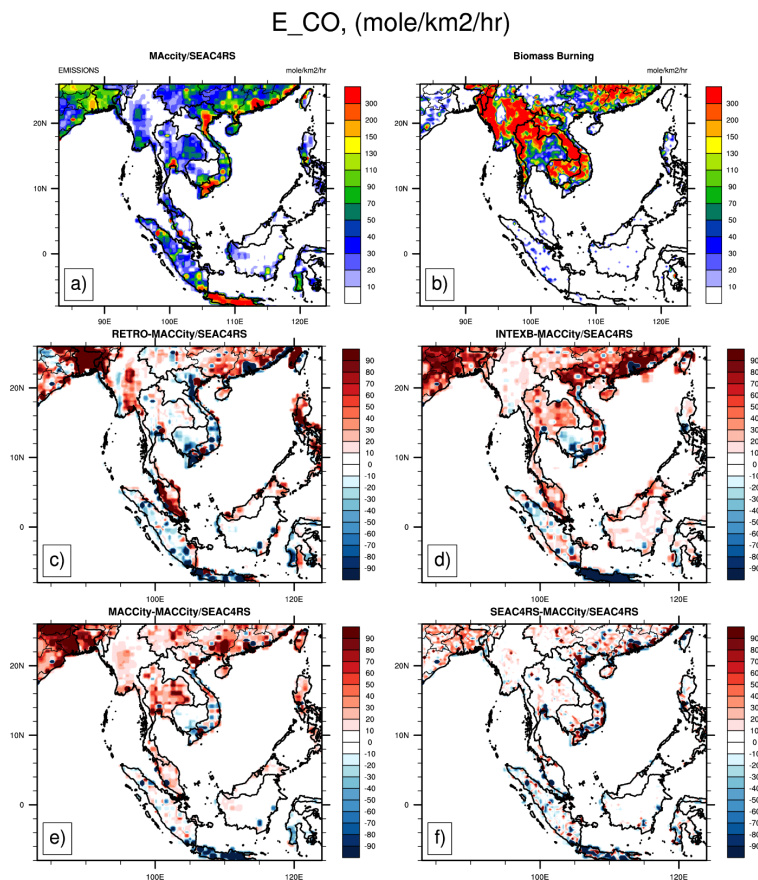


Fig. 1. Carbon monoxide emissions for March 2008 from different emission inventories (a) MACCity/SEAC4RS, (b) Biomass Burning, (c) RETRO-MACCity/SEAC4RS, (d) INTEXB-MACCity/SEAC4RS, (e) MACCity-MACCity/SEAC4RS, and (f) SEAC4RS-MACCity/SEAC4RS.

Effect of different emission inventories

T. Amnuaylojaroen et al.

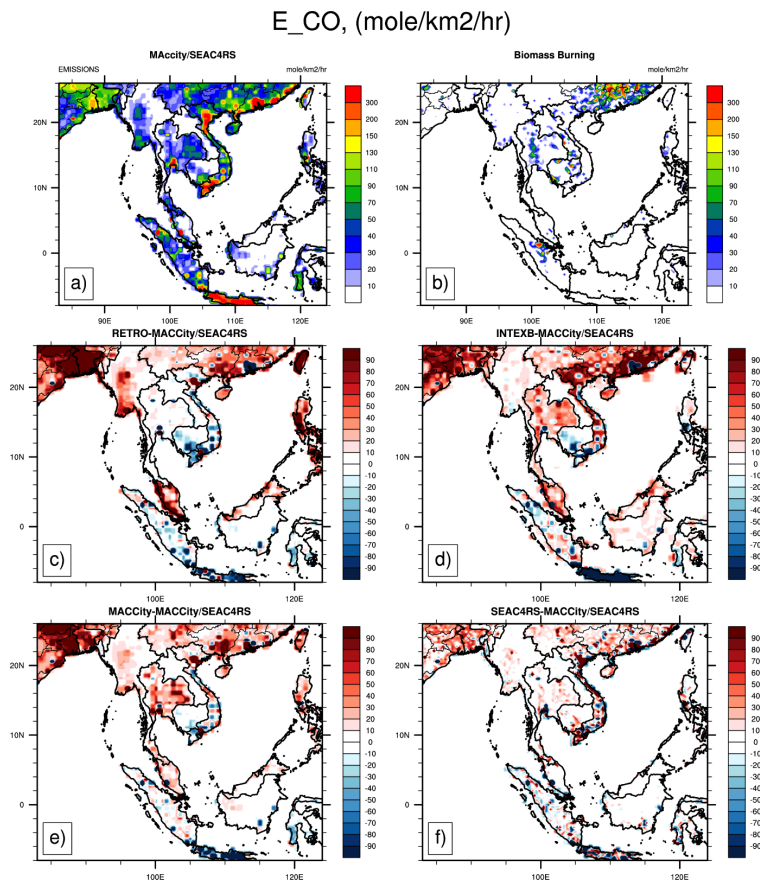


Fig. 2. Carbon monoxide emissions for December 2008 from different emission inventories **(a)** MACCity/SEAC4RS, **(b)** Biomass Burning, **(c)** RETRO-MACCity/SEAC4RS, **(d)** INTEXB-MACCity/SEAC4RS, **(e)** MACCity-MACCity/SEAC4RS, and **(f)** SEAC4RS-MACCity/SEAC4RS.

Title Page

Abstract

Introduction

Conclusions

References

Tables

Figures

◀

▶

◀

▶

Back

Close

Full Screen / Esc

Printer-friendly Version

Interactive Discussion



Effect of different emission inventories

T. Amnuaylojaroen et al.

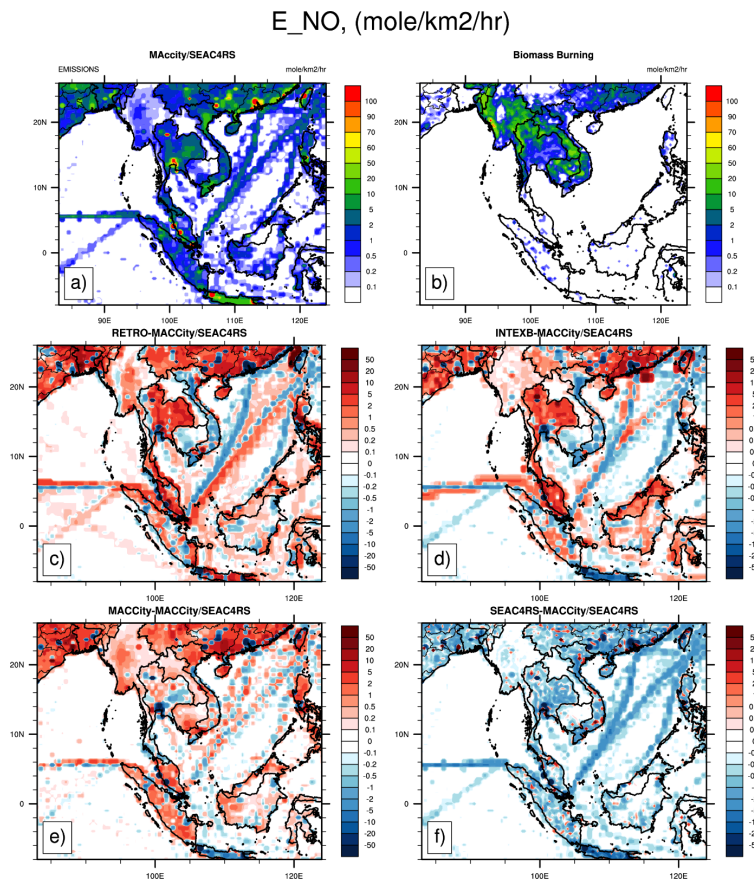


Fig. 3. Nitrogen oxides emissions for March 2008 from different emission inventories **(a)** MACCity/SEAC4RS, **(b)** Biomass Burning, **(c)** RETRO-MACCity/SEAC4RS, **(d)** INTEXB-MACCity/SEAC4RS, **(e)** MACCity-MACCity/SEAC4RS, and **(f)** SEAC4RS-MACCity/SEAC4RS.

Effect of different emission inventories

T. Amnuaylojaroen et al.

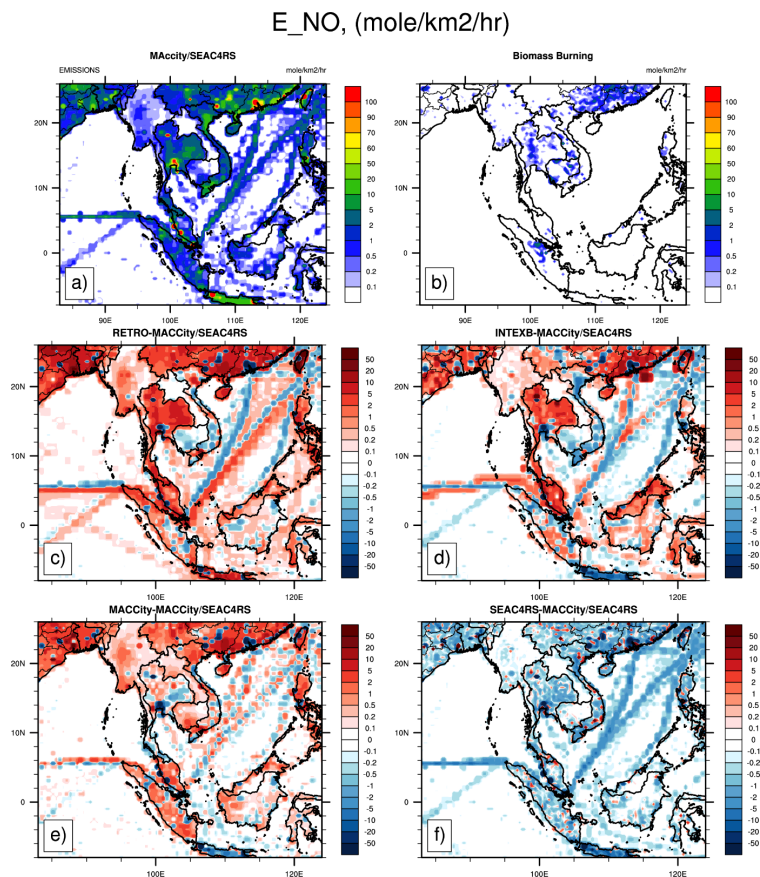


Fig. 4. Nitrogen oxides emissions for December 2008 from different emission inventories **(a)** MACCity/SEAC4RS, **(b)** Biomass Burning, **(c)** RETRO-MACCity/SEAC4RS, **(d)** INTEXB-MACCity/SEAC4RS, **(e)** MACCity-MACCity/SEAC4RS, and **(f)** SEAC4RS-MACCity/SEAC4RS.

Effect of different emission inventories

T. Amnuaylojaroen et al.

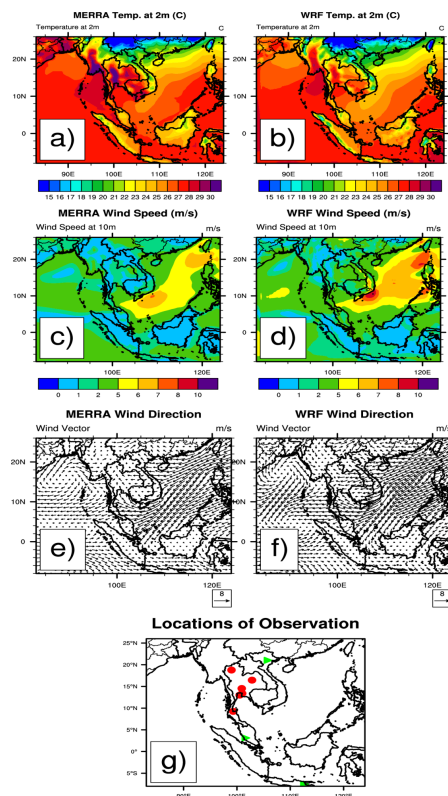


Fig. 5. March 2008 monthly-averaged **(a)** 2 m temperature ($^{\circ}\text{C}$) from MERRA, **(b)** 2 m temperature ($^{\circ}\text{C}$) from WRF, **(c)** 10 m wind speed (m s^{-1}) from MERRA, **(d)** 10 m wind speed (m s^{-1}) from WRF, **(e)** 10 m wind direction from MERRA, and **(f)** 10 m wind direction from WRF. **(g)** Locations of ground-based CO and O₃ measurements (red dot) and ozonesonde sites (green triangle) are marked.

Effect of different emission inventories

T. Amnuaylojaroen et al.

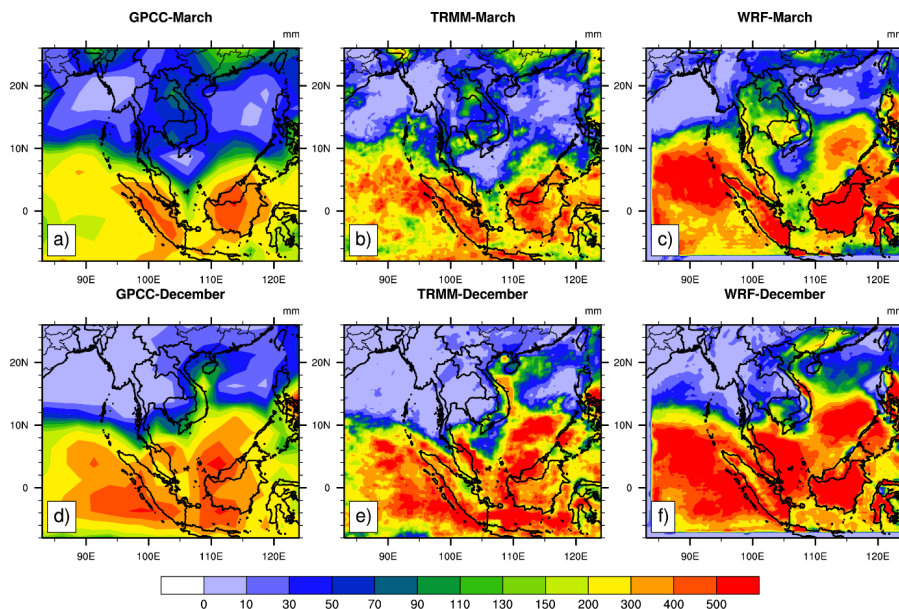


Fig. 6. Accumulated precipitation (mm) (a) GPCC, March, (b) TRMM, March and (c) WRF, March (d) GPCC, December (e) TRMM, December (f) WRF, December.

[Title Page](#)[Abstract](#)[Introduction](#)[Conclusions](#)[References](#)[Tables](#)[Figures](#)[◀](#)[▶](#)[◀](#)[▶](#)[Back](#)[Close](#)[Full Screen / Esc](#)[Printer-friendly Version](#)[Interactive Discussion](#)

Effect of different emission inventories

T. Amnuaylojaroen et al.

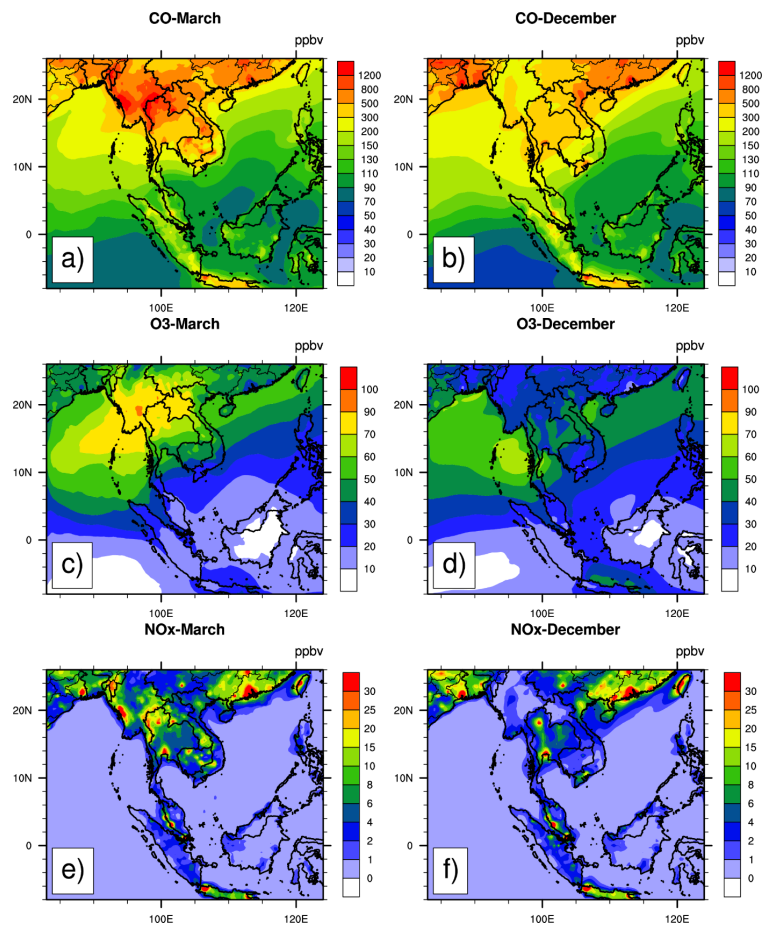


Fig. 7. Monthly-mean, surface mixing ratios for (a) and (b) CO, (c) and (d) for O₃, (e) and (f) for NO_x predicted by WRF-Chem using the averaged from 5 emission inventories for March (left) and December (right panels) 2008.

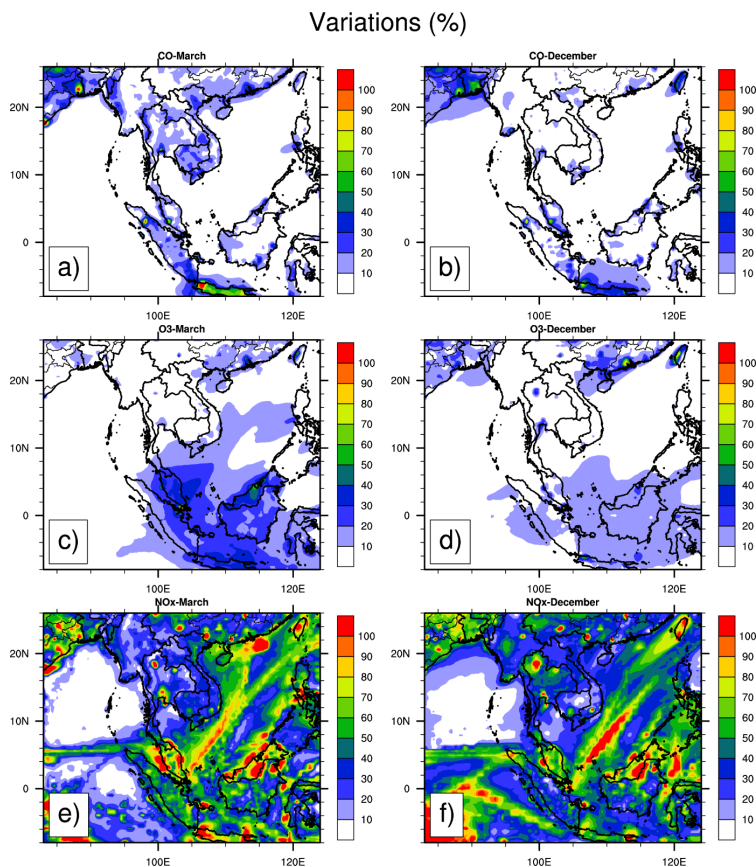


Fig. 8. Variations in surface mixing ratios for (a) and (b) CO, (c) and (d) O₃, (e) and (f) NO_x predicted by WRF-Chem using the averaged from 5 emission inventories for March (left) and December (right panels) 2008.

Effect of different emission inventories

T. Amnuaylojaroen et al.

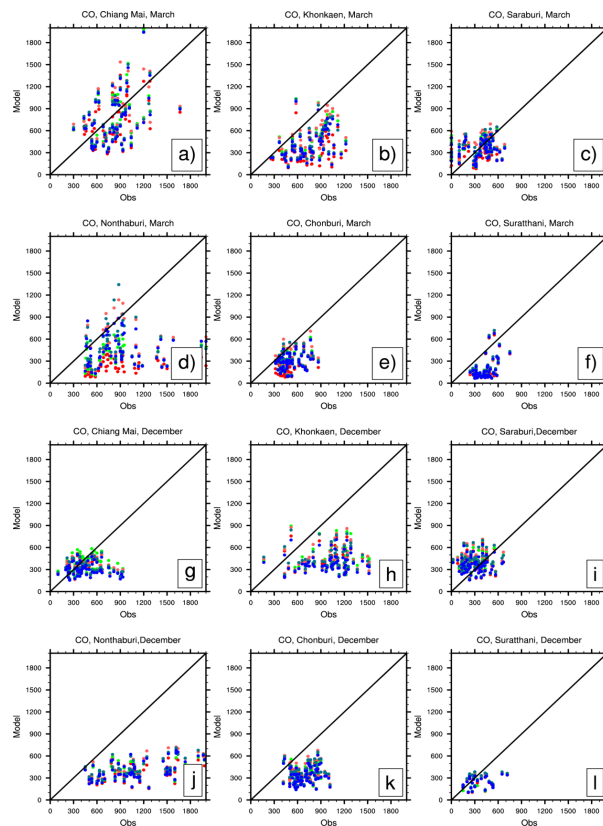


Fig. 9. Scatter plots of 6-hourly daytime CO from WRF-Chem using different emissions inventories (red dots are RETRO emissions, teal dots are SEAC4RS, orange dots MACCcity, green dots INTEX-B, and blue dots are combined MACCcity and SEAC4RS) and ground-based observations for March and December.

Effect of different emission inventories

T. Amnuaylojaroen et al.

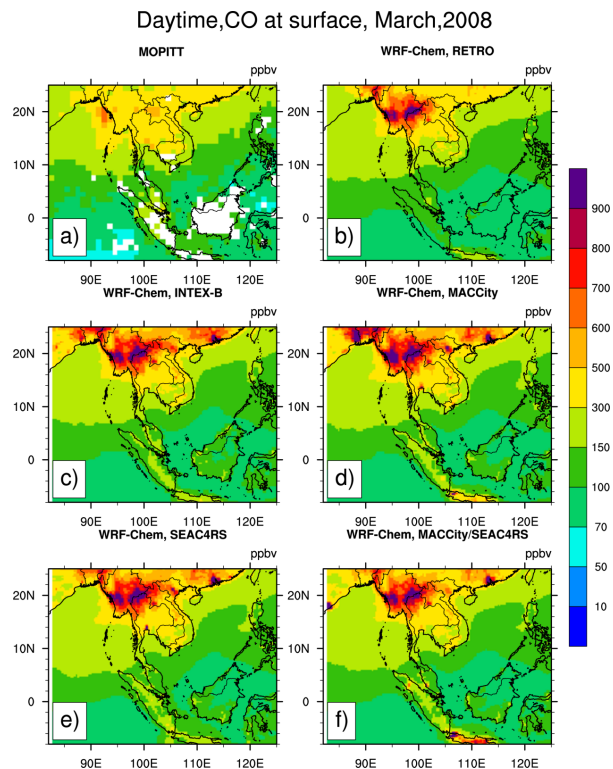


Fig. 10. Carbon monoxide from WRF-Chem and MOPITT in March **(a)** MOPITT **(b)** WRF-Chem Simulation with RETRO emission inventory, **(c)** WRF-Chem Simulation with INTEX-B emission inventory, **(d)** WRF-Chem Simulation with MACCity emission inventory, **(e)** WRF-Chem Simulation with SEAC4RS emission inventory, **(f)** WRF-Chem Simulation with MACCity/SEAC4RS emission inventory.

Daytime, CO at surface, December, 2008

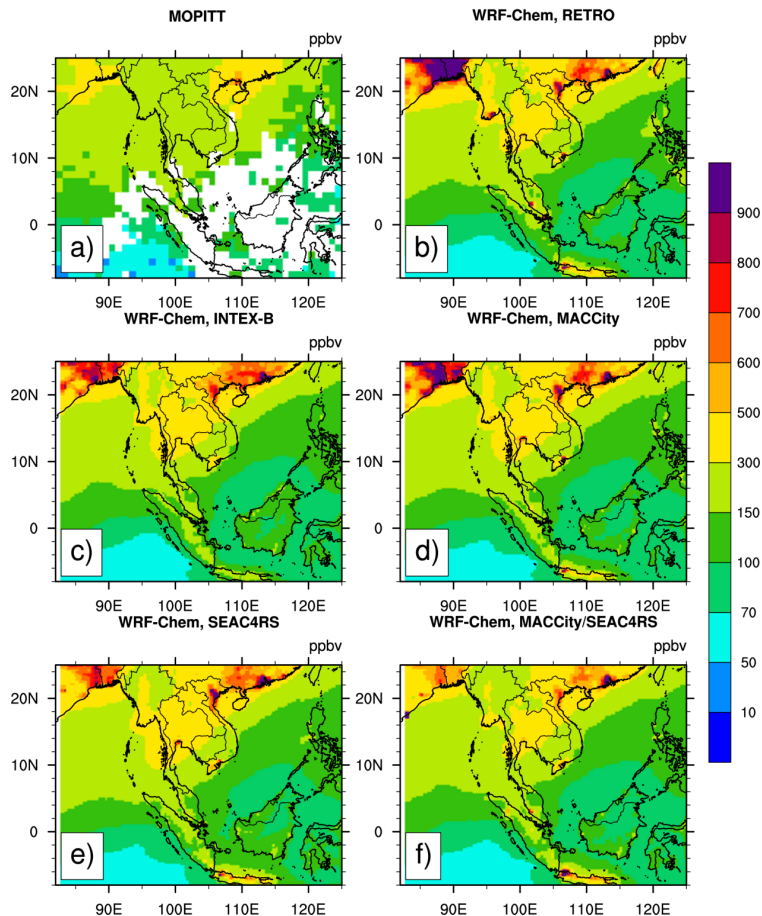


Fig. 11. Same as Fig. 10 but for December.

Effect of different emission inventories

T. Amnuaylojaroen et al.

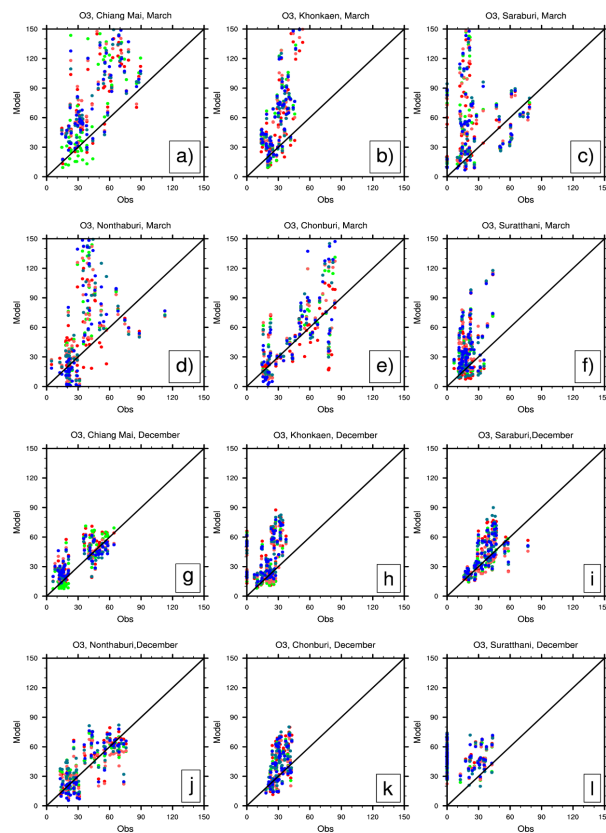


Fig. 12. Scatter plots of 6-hourly daytime ozone from WRF-Chem using different emissions inventories (red dots are RETRO emissions, teal dots are SEAC4RS, orange dots MACCcity, green dots INTEX-B, and blue dots are combined MACCcity and SEAC4RS) and ground-based observations for March and December.

[Title Page](#)[Abstract](#)[Introduction](#)[Conclusions](#)[References](#)[Tables](#)[Figures](#)[◀](#)[▶](#)[◀](#)[▶](#)[Back](#)[Close](#)[Full Screen / Esc](#)[Printer-friendly Version](#)[Interactive Discussion](#)

Effect of different emission inventories

T. Amnuaylojaroen et al.

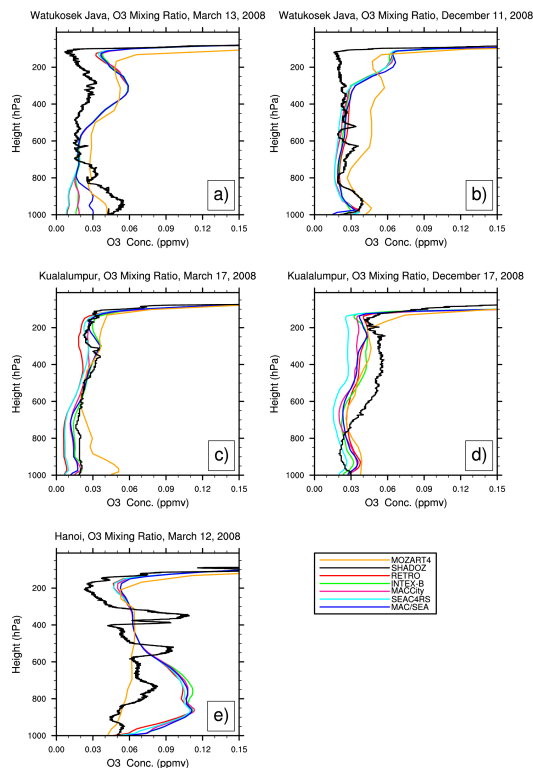


Fig. 13. Ozone vertical profiles from WRF-Chem, MOZART4, and ozonesondes at three SHADOZ ozonesonde locations for **(a)** Watukosek-Java, Indonesia in March, **(b)** Watukosek-Java, Indonesia in December, **(c)** Kuala Lumpur, Malaysia in March, **(d)** Kuala Lumpur, Malaysia in December, and **(e)** Hanoi, Vietnam in March. Note that there are no SHADOZ data at Hanoi during December 2008.

Title Page

Abstract

Introduction

Conclusions

References

Tables

Figures

◀

▶

◀

▶

Back

Close

Full Screen / Esc

Printer-friendly Version

Interactive Discussion



Monthly NO₂ Total Column (molecule/cm²), March

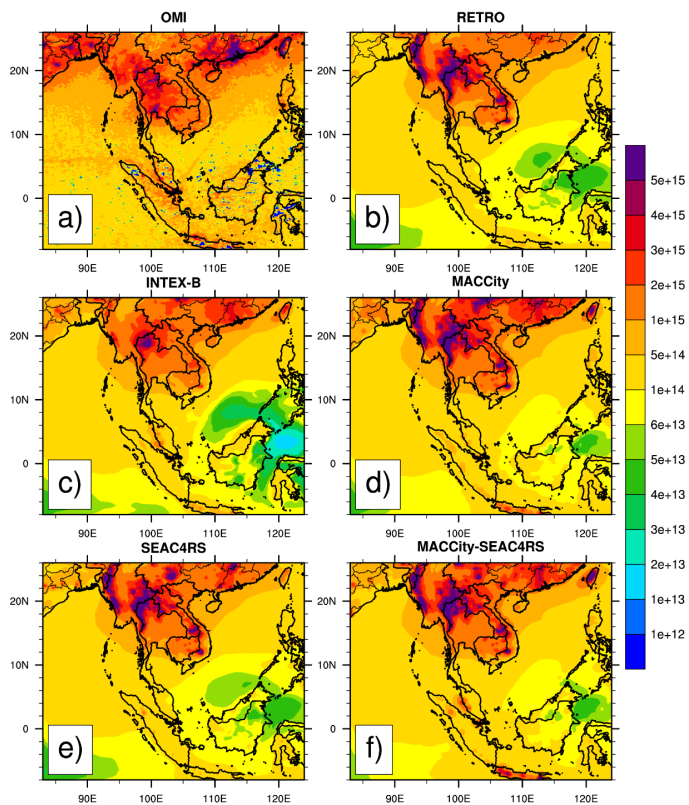


Fig. 14. March 2008 monthly NO₂ total column (a) OMI (b) WRF-Chem + RETRO (c) WRF-Chem + INTEX-B (d) WRF-Chem + MACCity (e) WRF-Chem + SEAC4RS (f) WRF-Chem + MACCity-SEAC4RS.

Monthly NO₂ Total Column (molecule/cm²), December

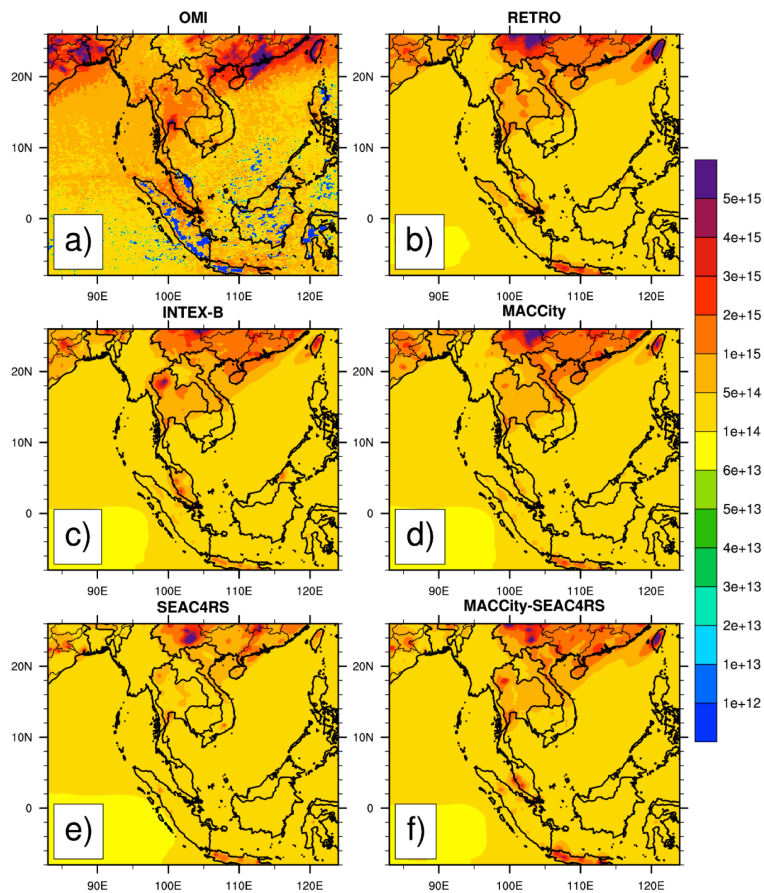


Fig. 15. Same as Fig. 14 but for December.

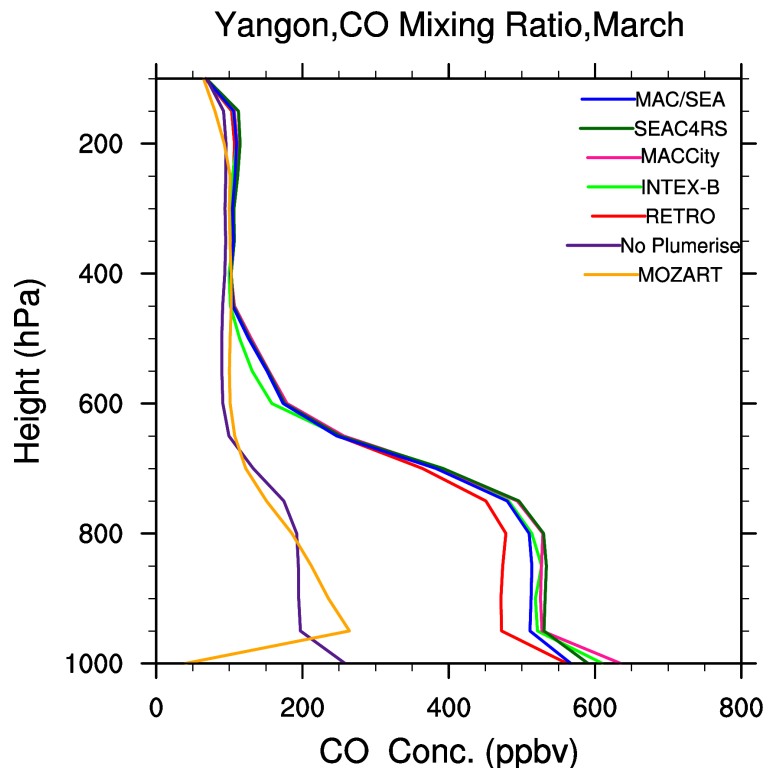


Fig. 16. March monthly-averaged CO vertical profiles at Yangon, Burma. WRF-Chem results with the plumerise feature of biomass burning emissions are given for the MACCity/SEAC4RS emissions case (blue line), SEAC4RS emissions (dark green line), MACCity emissions (red line), INTEX-B emissions (green line), and RETRO emissions (dark red line). The MOZART global model results are shown as the gold line. WRF-Chem results without the plumerise feature (i.e. biomass burning emissions injected into the lowest model level) are shown as the purple line.

[Title Page](#)[Abstract](#)[Introduction](#)[Conclusions](#)[References](#)[Tables](#)[Figures](#)[◀](#)[▶](#)[◀](#)[▶](#)[Back](#)[Close](#)[Full Screen / Esc](#)[Printer-friendly Version](#)[Interactive Discussion](#)